A Biased Random Walk Model for the Trajectories of Swimming Micro-organisms

N. A. HILL* AND D.-P. HÄDER†

* *Department of Applied Mathematical Studies*, *University of Leeds*, *Leeds LS2 9JT*, *England*; and † *Institut für Botanik und Pharmazeutische Biologie*, *Universität Erlangen-Nürnberg*, *Staudtstrasse* 5, *D*-91058, *Erlangen*, *Germany*

The motion of swimming micro-organisms that have a preferred direction of travel, such as single-celled algae moving upwards (gravitaxis) or towards a light source (phototaxis), is modelled as the continuous limit of a correlated and biased random walk as the time step tends to zero. This model leads to a Fokker–Planck equation for the probability distribution function of the orientation of the cells, from which macroscopic parameters such as the mean cell swimming direction and the diffusion coefficient due to cell swimming can be calculated. The model is tested on experimental data for gravitaxis and phototaxis and used to derive values for the macroscopic parameters for future use in theories of bioconvection, for example.

© 1997 Academic Press Limited

1. Introduction

It is well known that suspensions of swimming micro-organisms, such as the alga *Chlamydomonas nivalis*, form cooperative patterns on lengthscales of the order of millimetres, which are much greater than the size of the individual cells. In order to understand the fluid dynamics of these macroscopic patterns, the suspension has been modelled mathematically as a continuum, see e.g. Childress *et al*. (1975), Pedley *et al*. (1988) and Hill *et al*. (1989). An important feature of such models is the prescription of both a preferred direction of swimming, influenced for example by gravity (positive or negative gravitaxis) or by light (phototaxis), and at the same time a degree of "randomness" in the behaviour of individuals and across the whole population of micro-organisms. It is of fundamental importance, therefore, that we understand how the motion of individuals ultimately contributes to the bulk flux of cells. Secondly, it is of intrinsic interest to analyse and quantify the motion of individual cells and thus to identify differences in behaviour, which arise either as a result of environmental changes or between different samples.

In this paper, we present a statistical theory in which we model, in as general a way as possible, the motion of the cells as the continuous limit of a correlated and biased random walk as the time step tends to zero. The walk is correlated because the cells change direction gradually and biased because there is a preferred direction of motion. We have carried out experiments on *C. nivalis* and *Peridinium gatunense* in which we have recorded the trajectories of individual cells in a sample of the suspension, and we are able to demonstrate that the theory is self-consistent and to derive quantitative measurements of the micro-organisms' motion. A further complication is that it has been necessary to collect the data as projections onto vertical and horizontal planes, and so we also show how to analyse the projected trajectories.

Pedley & Kessler (1990) have derived a model for the motion of individual micro-organisms subject to gyrotaxis, which combines deterministic torque balances on a cell with rotational diffusion. We are able to measure the key parameters in their model directly. The results of our theories should provide a

basis for future analysis of more complicated systems, e.g. when there are several competing external influences.

In earlier work on *Escherichia coli*, Berg & Brown (1972) were able to track single, isolated bacteria in three dimensions and show that their motion consists of a series of almost straight runs followed by a short time spent tumbling before setting off in another straight line in a different direction. This behaviour is markedly different to that of the algae studied here, whose direction varies continuously and smoothly. Lovely & Dahlquist (1975) used a random walk model to describe the motion of *E. coli* when the motion is isotropic (i.e. in the absence of a preferred direction) and they showed how to derive a diffusion coefficient for the flux of bacteria. They also discussed some bulk statistical measures when there is a preferred direction, but they did not link this directly to a random walk model for the individual cells. Thus, our work extends both the theoretical and the experimental work on *E. coli*.

The paper is organized as follows. In Section 2, we describe our experimental techniques and introduce typical cell trajectories as a motivation for theory which follows in Sections 3 to 8. The behaviour of cells which are oriented by gravitaxis and by phototaxis is reviewed in Section 9. In Section 10 and Section 11, we present our experimental results, and end with a discussion in Section 12.

2. Experimental Methods

The unicelluar photosynthetic freshwater flagellate *Chlamydomonas nivalis* (Willie CCAP 11/51) was grown by inoculating 1 ml of a logarithmic phase culture into 40 ml of Bold's basal medium (Bold & Wynne, 1978) contained in 100-ml Erlenmeyer flasks. The cultures were kept for about 6 weeks under continuous light of about 600 lux ($=2.5$ W m^{-2} from mixed cool white and warm tone fluorescent lamps, Osram 136 W/32) at 23°C. The experiments were carried out with the cells in their original growth medium. Cultures of the armoured, fresh water dinoflagellate *Peridinium gatunense* were also grown in a medium described by Lindström (1982) under the same conditions.

Measurements on the cell suspensions were taken in a flat cuvette of $40 \times 8 \times 0.17$ mm^3 inner dimensions that was held on the stage of a conventional light microscope (Zeiss Standard, Oberkochen, Germany). For observations of cells swimming in a vertical plane, the microscope was placed on its side so that the optical axis was horizontal. During experiments, an actinic white light beam was produced from a

250-W quartz halogen slide projector (Prado, Leitz, Wetzlar, Germany), the beam of which was collimated with a 200-mm focal-length lens and an infrared cut-off filter. The irradiance was controlled by inserting neutral density filters (Schott & Gen., Mainz, Germany) and measured at the position of the cuvette using a luxmeter (Mavolux, Gossen, Erlangen, Germany).

The motion of the organisms was tracked using a real-time image analysis system as described by Häder & Lebert (1985). The images of the swimming cells were recorded with an infrared-sensitive video camera (Sony AVC 3250). The video images were digitized in real time with a resolution of 256×256 pixels with 64 gray levels and stored in RAM (random access memory). The system grabs an initial frame and searches it to identify one organism at random according to preselected size and greyscale parameters. Having found a cell, the software determines the cell's outline and calculates its centroid and the time. After finding the cell's position, the next image is digitized and the new image of the cell is sought. If successful, the new time and position of the centroid are calculated and recorded, and the process is repeated. If unsuccessful, a new cell is sought and the whole process is repeated. Fixed time steps are not used because the computational time between images varies slightly, but the mean, $\bar{\tau}$, and standard deviation (s.d.), σ_τ, of the time steps are 0.08 s and 0.01 s, respectively. The population of cells is observed over 5 or 10 minutes so that several hundred tracks can be recorded. In practice, the data consists of relatively short trajectories from many cells and the
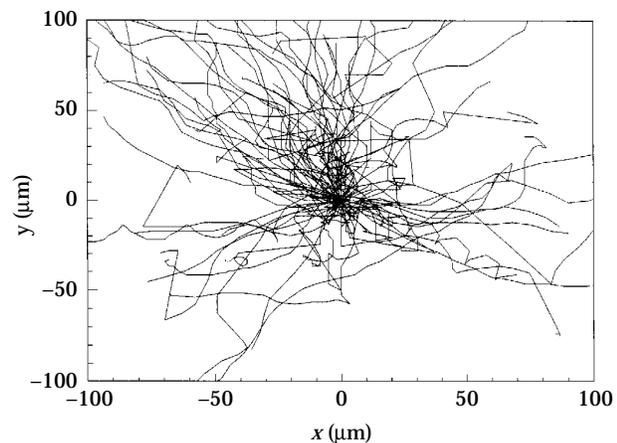

FIG. 1. A sample of swimming trajectories of *C. nivalis* cells, recorded in a vertical plane. The origin of each trajectory has been moved to the centre of the diagram so that they can be compared with each other more easily. The trajectories are clustered around the upper vertical axis showing that the cells are negatively gravitactic. Note that they change direction gradually and do not run-and-tumble like bacteria such as *E. coli*.

effects of interactions are included in the data. Plots of typical trajectories are shown in Fig. 1.

One serious difficulty in the sort of experiments described here is the occurrence of drifts due to thermal convection currents within the cuvette containing the suspension. A thin cuvette of depth 0.17 mm was used but it is very difficult to eliminate such fluid motion completely; even in a laboratory with very good temperature control there are always local sources of heat. In particular, the light sources used to visualize the cells and to induce phototaxis always produce radiation that is absorbed by the fluid and the swimming cells, even after careful filtering. Furthermore, flows in the suspension induce fluid shear, which also contributes to the passive orientation of cells and, in fact, plays a major role in the orientation of cells by gyrotaxis, which leads directly to the formation of plumes in bioconvection (Kessler, 1986). Although the ideal is to eliminate completely convection in these experiments, which does not appear to be feasible, some experiments have been carried out, in which easily identifiable, passively advected particles were introduced into the suspension so that the drifts could be measured. It was found that such thermal currents did not usually exceed about $10~\mu\mathrm{m~s^{-1}}$.

3. Circular Statistics

In this section we briefly review the elements of circular and spherical statistics that are needed for the random walk model and data analysis. For further details, the reader is referred to the books by Mardia (1972) and Batschelet (1981). Given a set of angles $\{\theta_i\}_{i=1}^n$, representing for example the orientation of directed segments of lines (i.e. vectors) in a plane, the circular sample mean ϕ and mean length r are defined by

$$r\cos\phi = \sum_{i=1}^n \cos\theta_i/n, \quad r\sin\phi = \sum_{i=1}^n \sin\theta_i/n,$$

where $-\pi \leqslant \phi < \pi$ and clearly $0 \leqslant r \leqslant 1$. The mean length provides a useful measure of how closely distributed the set of angles is; when r is close to one the distribution of angles is sharply peaked, and when r is close to zero the distribution is almost uniform. By analogy with the standard deviation in linear statistics, we can define the angular deviation s to be

$$s = \sqrt{2(1-r)}$$

and then s^2 is the circular variance. An alternative

definition of the angular deviation is

$$s_0 = \sqrt{-2\ln r}, \tag{1}$$

which arises from the analogy between a circular distribution called the wrapped normal distribution and the normal distribution of linear statistics, as we shall show later. Both s and s_0 tend to the same limit, zero, as r tends to one but s_0 becomes infinite as r tends to zero.

Probability distribution functions $f(\theta)$ on a circle (and their equivalents on a sphere) satisfy

$$f(\theta) \geqslant 0 \ \forall \ -\pi \leqslant \theta < \pi \tag{2}$$

and the normalization condition that the total probability is one i.e.

$$\int_{-\pi}^{\pi} f(\theta)\,\mathrm{d}\theta = 1. \tag{3}$$

Corresponding to the moments of a linear probability distribution function (p.d.f.), the angular or trigonometric moments are defined as the Fourier coefficients

$$a_n = \int_{-\pi}^{\pi} \cos(n\theta)f(\theta)\,\mathrm{d}\theta, \quad b_n = \int_{-\pi}^{\pi} \sin(n\theta)f(\theta)\,\mathrm{d}\theta$$

$$\forall \ n = 1, 2, 3, \ldots \tag{4}$$

The polar forms of these moments are written as ρ_n and ϕ_n where

$$\rho_n \exp(i\phi_n) = a_n + ib_n. \tag{5}$$

ρ_1 and ϕ_1 are simply interpreted as the mean length and mean angle of the distribution. The following three distributions are particularly useful.

(A) THE UNIFORM DISTRIBUTION

When the distribution is uniform, points are distributed with equal probability over the circle and

$$f(\theta) = U(\theta) \equiv 1/2\pi.$$

For the uniform distribution, $\rho_1 = 0$, ϕ is undefined and $s = \sqrt{2}$.

(B) THE VON MISES DISTRIBUTION

The von Mises distribution is a unimodal distribution defined by

$$f(\theta) = M(\theta; \mu, \kappa) \equiv \frac{1}{2\pi I_0(\kappa)} \exp[\kappa\cos(\theta - \mu)], \tag{6}$$

where the parameter μ is the mean angle and the κ is the concentration parameter. $\kappa \geqslant 0$. I_0 is a modified Bessel's function of the first kind and zeroth order. The von Mises distribution equals the uniform distribution when $\kappa = 0$, and becomes sharply peaked

as $\kappa \to \infty$. For the von Mises distribution, $\phi_1 = \mu$ and $\rho = A(\kappa)$, where

$$A(\kappa) = I_1(\kappa)/I_0(\kappa) \qquad (7)$$

which is readily calculated numerically and tabulated (Batschelet, 1981; Mardia, 1972).

(C) THE WRAPPED NORMAL DISTRIBUTION

As its name implies, the wrapped normal distribution is the linear normal distribution wrapped around the unit circle. It too is unimodal and defined by

$$f(\theta) = W(\theta; \mu, \sigma)$$

$$\equiv \frac{1}{\sigma\sqrt{2\pi}} \sum_{k=-\infty}^{k=\infty} \exp[-(\theta - \mu + 2\pi k)^2/2\sigma^2], \qquad (8)$$

where μ and $\sigma > 0$ are parameters. For the wrapped normal distribution, $\rho_1 = \exp(-\sigma^2/2)$ and $\phi_1 = \mu$. For this distribution,

$$\sigma = \sqrt{-2 \ln \rho_1} \qquad (9)$$

which motivates the alternative definition (1) of the angular deviation. It is helpful to note that when σ is related to κ by

$$A(\kappa) = \exp(-\sigma^2/2), \qquad (10)$$

the von Mises and wrapped normal distributions differ by only a few percent so that in applications it is convenient to treat their properties as being indistinguishable because the trigonometric moments of the wrapped normal distribution are simpler to calculate than those of the von Mises distribution, whereas the maximum likelihood estimators of the von Mises distribution are much simpler to compute than those of the wrapped normal distribution.

(D) MAXIMUM LIKELIHOOD ESTIMATORS

The sample mean ϕ is an unbiased, maximum likelihood estimator for the mean angle ϕ_1 for all the distributions. The mean length r is a maximum likelihood estimator for ρ_1 only for the von Mises distribution but it is heavily biased and over-estimates κ. If n is the number of data points, an approximate rule to correct this (Batschelet, 1981) is given by

$$r \leqslant 1/\sqrt{n} \Rightarrow \kappa = 0, \qquad (11)$$

$$r > 1/\sqrt{n} \Rightarrow \kappa \text{ is the root of } A(\kappa) = rA(nr\kappa). \quad (12)$$

(E) CORRECTION FOR GROUPING

When circular or angular statistics are analysed, the data are often grouped into a number, k say, of bins of a width, $\lambda = 2\pi/k$. Let n_i be the number of points in the i-th bin and let $\phi^{(i)}$ be the midpoint of the i-th bin. The sample mean angle and length are then given by

$$r \cos \phi = \sum_{i=1}^{k} n_i \cos \phi^{(i)} \Big/ \sum_{i=1}^{k} n_i, \qquad (13)$$

$$r \sin \phi = \sum_{i=1}^{k} n_i \sin \phi^{(i)} \Big/ \sum_{i=1}^{k} n_i. \qquad (14)$$

No correction is needed for the sample mean but the mean length is biased and tends to be a little too small. The corrected mean length r_c is given by

$$r_c = r\lambda/2 \sin(\lambda/2). \qquad (15)$$

In this paper, only one width, $\pi/6$, of bins is used for which $r_c = 1.0115r$. The corrected value of the angular deviation is

$$s_c = \sqrt{2(1 - r_c)}. \qquad (16)$$

4. The Random Walk on a Circle

Suppose that the motion of a cell moving in a plane is such that the probability distribution function (p.d.f.) for the speed is independent of the p.d.f. for the direction of travel. Suppose also that the motion can be modelled as a random walk in which a cell changes its velocity at certain instants in time, t_i. The random walk or trajectory is specified by the set of points $\{(x_i, t_i)\}_i^n = 0$, where $x_i = (x_i, y_i)$ is the position vector with respect to the fixed laboratory frame of reference. A segment of the trajectory is defined as the straight line joining any two consecutive points and the absolute directions $\{\theta_i\}_{i=1}^n$ of the segments are given by

$$\cos \theta_i = \mathbf{k}.(x_i - x_{i-1})/|x_i - x_{i-1}| \ \forall \ i = 1, 2, \ldots, n,$$

where $\mathbf{k}$ is a unit vector parallel to a reference direction in the plane (upwards if the plane is vertical) and $-\pi \leqslant \theta_i < \pi$. If we consider only the direction of travel because the speed is an independent random variable, then the points $\{\theta_i, t_i\}_i^n = 1$ can be thought of as a random walk on the unit circle and we seek to derive the p.d.f. for θ, $f(\theta)$, and the circular moments of θ. If there is a preferred direction, denoted by θ_0, then the walk is said to be biased.

A second important random variable is the set of turning angles $\{\delta_i\}_{i=2}^n$ defined by

$$\delta_i = \theta_i - \theta_{i-1}, \ -\pi \leqslant \delta_i < \pi \ \forall \ i = 2, \ldots, n. \quad (17)$$

This too describes a random walk on the unit circle. If the original random walk in the plane is biased then δ is a function of θ. A random walk is said to be correlated if a_1, the mean cosine defined in eqn (4), is strictly positive i.e. at each time step there is a tendency to continue to travel in the same direction.

These definitions and concepts are easily extended to motion in a volume of space, in which $\mathbf{x}_i = (x_i, y_i, z_i)$ and θ and δ are replaced by pairs of Euler angles leading to random walks on the unit sphere.

5. The Fokker–Planck Equation

In order to derive the p.d.f. for θ, we consider the continuous limit of the random walk on a circle. Here we present a heuristic argument for the derivation. For further details see Cox & Miller (1965) and Risken (1989). Suppose that there is a small, fixed time step τ between changes in direction and that at time t the direction equals $\theta(t)$. At time $t + \tau$, the direction either changes by a small angle $\pm \delta$ or is unchanged with probabilities given by

$$P(\delta) = p(\theta), \quad P(-\delta) = q(\theta),$$
$$P(0) = 1 - p(\theta) - q(\theta), \tag{18}$$

where $p(\theta)$ and $q(\theta)$ are small, continuous functions of θ. Then, drawing the proper distinction between the random variable Θ and its value θ, we define the p.d.f. $f(\theta, t)$ of Θ by

$$f(\theta, t)\delta = P[\theta \leqslant \Theta(t) < \theta + \delta]. \tag{19}$$

On considering the previous time step, we see that

$$f(\theta, t) = f(\theta - \delta, t - \tau)p(\theta - \delta)$$
$$+ f(\theta, t - \tau)[1 - p(\theta) - q(\theta)]$$
$$+ f(\theta + \delta, t - \tau)q(\theta + \delta). \tag{20}$$

We expand the last equation in a Taylor series and take the limit as τ and δ tend to zero, retaining terms $O(\tau)$, $O(\delta)$ and $O(\delta^2)$. To do this, we require that

$$E[\Theta(t + \tau) - \Theta(t)] \equiv E[\Delta(\theta, \tau)] \equiv \mu_\delta(\theta, \tau) = \mu_0(\theta)\tau \tag{21}$$

and

$$\mathrm{Var}[\Theta(t + \tau) - \Theta(t)] \equiv \mathrm{Var}[\Delta(\theta, \tau)]$$
$$\equiv \sigma_\delta^2(\theta, \tau) = \sigma_0^2(\theta)\tau \tag{22}$$

asymptotically as $\tau \to 0$, where

$$\Delta(\theta, \tau) = \Theta(t + \tau) - \Theta(t) \tag{23}$$

is the random variable corresponding to the turning angle. Note that for convenience we shall use the notation μ_δ and σ_δ to denote the expectation and angular deviation of $\Delta(\theta, \tau)$ henceforth. These conditions on the mean and variance of $\Delta(\theta, \tau)$ can be satisfied if

$$p(\theta) = [\sigma_0^2(\theta) + \mu_0(\theta)\delta]/2A,$$
$$q(\theta) = [\sigma_0^2(\theta) - \mu_0(\theta)\delta]/2A$$

and

$$\delta^2 = A\tau \quad \text{as} \quad \tau \to 0,$$

where A is a positive constant such that $\sigma_0^2(\theta) < A$. Taking this limit yields the Forward Kolmogorov or Fokker–Planck equation for $f(\theta, t)$

$$\frac{\partial}{\partial t}f(\theta, t) = -\frac{\partial}{\partial \theta}[\mu_0(\theta)f(\theta, t)]$$
$$+ \frac{1}{2}\frac{\partial^2}{\partial \theta^2}[\sigma_0^2(\theta)f(\theta, t)]. \tag{24}$$

Thus, when we are approximating a swimming cell's trajectory by the continuous limit of a random walk, we need to demonstrate that the distribution of the turning angle, Δ, tends to the correct limits (21) and (22) as the time step is decreased, in which case we have direct measurements of the coefficients in the Fokker–Planck equation (24), which are needed to calculate $f(\theta, t)$ and hence the macroscopic mean cell velocity and cell diffusivity used in continuum models of suspensions of motile micro-organisms. We refer to $\mu_0(\theta)$ as the orientation (or drift) coefficient for the Fokker–Planck equation and

$$D = \sigma_0^2/2 \tag{25}$$

as the effective rotational diffusivity for the cells.

The Fokker–Planck equation (24) is solved subject to the conditions that $f(\theta, t)$ and the probability flux

$$j(\theta, t) \equiv \mu_0(\theta)f(\theta, t) - \frac{1}{2}\frac{\partial}{\partial \theta}[\sigma_0^2(\theta)f(\theta, t)] \tag{26}$$

are both periodic, specifically that

$$f(-\pi, t) = f(\pi, t) \quad \text{and} \quad j(-\pi, t) = j(\pi, t) \tag{27}$$

for all $t > 0$. In addition, $f(\theta, t)$ must be non-negative (2) and normalized (3) and, for the time-dependent problem, satisfies a suitable initial condition. All the solutions of (24) ultimately decay to a steady-state independent of the initial conditions, which is the state that we expect to observe in the experiments described further on.

6. Models for Reorientation

In this section, motivated by observations on swimming cells, we consider two possible models for the orientation or drift coefficient $\mu_0(\theta)$ [see eqn (21)] and calculate the steady solutions of the Fokker–Planck equation (24). In both cases, we take $\sigma_0(\theta)$, which is difficult to measure in practice, to be a constant and determine the relationship between it and the angular, deviation, σ_θ, of the steady solution of (24), which is more easily measured. These results are needed below in the analysis of the data.

6.1. SINUSOIDAL REORIENTATION

Suppose that the orientation coefficient takes the form

$$\mu_0(\theta) = -d_0 \sin(\theta - \theta_0) \quad (-\pi \leqslant \theta, \theta_0 < \pi), \quad (28)$$

where θ_0 is a constant corresponding to the preferred direction and d_0 is the amplitude of the drift coefficient and is taken to be a positive constant. When σ_0 is also a constant, the normalized solution of the steady Fokker–Planck equation (24) plus boundary conditions is easily shown to be the von Mises distribution

$$f(\theta) = M(\theta; \theta_0, 2d_0/\sigma_0^2) \quad (29)$$

[see eqn (6)]. From (1) and (7), it follows that the angular deviation of this von Mises distribution (29) is

$$\sigma_\theta = \sqrt{-2 \ln[A(2d_0/\sigma_0^2)]}. \quad (30)$$

Thus given independent measurements of d_0 and σ_θ, (30) can be inverted to give

$$\sigma_0 = \sqrt{2d_0/A^{-1}[\exp(-\sigma_\theta^2/2)]}, \quad (31)$$

which is readily calculated using for example a Newton–Raphson numerical scheme to evaluate the inverse function A^{-1} or from tables of A^{-1}. In fact, the quickest method is to read off values of $A^{-1}(\kappa)$ from a graph of $A(\kappa)$ as this is sufficiently accurate for the data in this paper.

6.2. LINEAR REORIENTATION

A second model for the orientation coefficient is

$$\mu_0(\theta) = \begin{cases} -d_0\theta, & -\pi < \theta < \pi, \\ 0, & \theta = \pm\pi, \end{cases} \quad (32)$$

where again the amplitude, d_0, of the orientation coefficient is a positive constant. On taking σ_0 to be a positive constant, the normalized solution of the steady Fokker–Planck equation (24) plus boundary

conditions is readily shown to be

$$f(\theta) = B(\lambda) \exp(-\lambda\theta^2), \quad \lambda = d_0/\sigma_0^2, \quad (33)$$

where $B(\lambda)$ is the normalization function defined by

$$B(\lambda) = 1 \bigg/ \int_{-\pi}^{\pi} \exp(-\lambda\theta^2) \, \mathrm{d}\theta = \sqrt{\lambda}\bigg/\bigg(\sqrt{\pi} \, \mathrm{erf}(\pi\sqrt{\lambda})\bigg). \quad (34)$$

Note that $f(\theta)$ and the probability flux $j(\theta)$ are required to be continuous at $\theta = \pm\pi$, as specified in (27), but $\partial f/\partial \theta$ is not because $\mu(\theta)$ is discontinuous there. The mean length and angle of this distribution are

$$\rho = B(\lambda) \int_{-\pi}^{\pi} \cos(\theta) e^{-\lambda\theta^2} \, \mathrm{d}\theta,$$

$$\phi = B(\lambda) \int_{-\pi}^{\pi} \sin(\theta) e^{-\lambda\theta^2} \, \mathrm{d}\theta = 0, \quad (35)$$

respectively [see eqns (4) and (5)]. The angular deviation is

$$\sigma_\theta(\lambda) = \sqrt{-2 \ln \rho} \quad (36)$$

from definition (1). As for (30) above, this relationship is straightforward to invert to find σ_0 given values of σ_θ and d_0, and for this paper was most easily evaluated graphically by plotting $\sigma_\theta(\lambda)$ using numerical values for ρ.

7. Discretization of the Cells' Trajectories

7.1. THE DISCRETIZED RAW DATA

The image processor used in the experiments reported here has a resolution of 256×256 rectangular pixels which are 1.70 μm wide by 1.23 μm high on the real image. When the image is digitized, a random error in the cells' positions due to the finite resolution of the pixels is introduced. A particular analytical example of such discretization errors was discussed by Scharstein in Alt & Hoffmann (1990). In addition, the algorithm used to determine an individual cell's trajectory, first attempts to identify the edge of the cell and thence the position of the geometric centre, or centroid. Inaccuracies in the determination of the cell's boundary also contribute to the error in its position. In these experiments, as is shown below, a swimming cell moves about five pixels on average between data points so that the finite resolution is a significant source of error in the trajectory analysis. For the purposes of this paper, we
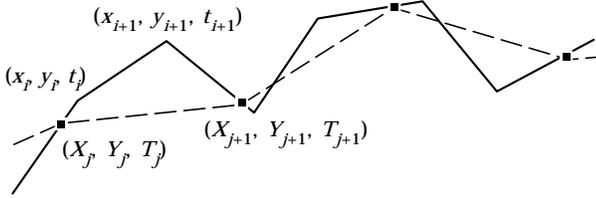
FIG. 2. A diagram to illustrate rediscretization of trajectories. The original trajectory (solid line) consists of data points (x_i, y_i) recorded at times t_i. This trajectory is rediscretized (dashed line) using linear interpolation to obtain a new set of data points (X_i, Y_i, T_i) with a uniform time step τ.

shall refer to the cumulative effects of all these errors as 'pixel noise'.

7.2. REDISCRETIZATION

The software algorithm for discretizing the cells' trajectories, records sets of positions and times as described in Section 2 above. The set of positions and times for any one cell, $\{x_i, y_i, t_i\}_{i=0}^{n}$ say, is rediscretized into a trajectory with uniform time steps τ by linear interpolation into the new set of points $\{X_i, Y_i, T_i\}_{i=0}^{N}$ using the following algorithm:

(1) $T_j = t_0 + j\tau \ \forall \ j = 0, 1, 2, \ldots$;

(2) $(X_0, Y_0, T_0) = (x_0, y_0, t_0)$;

(3) given (X_j, Y_j, T_j), find k such that

$$T_j + 1 = (1 - q)t_k + qt_{k+1},$$

where $0 \leqslant q < 1$, and then

$$(X_{j+1}, Y_{j+1}) = (1 - q)(x_k, y_k) + q(x_{k+1}, y_{k+1}).$$

(See Fig. 2.) When rediscretizing, the new time step τ should be greater than half of the experimental mean time step $\bar{\tau}/2$ to avoid spurious correlations in the data.

For values of $\tau > \bar{\tau}/2$, one effect of rediscretization is to smooth the apparent trajectory. Although there is no detailed theory available, we find that in practice for our data, when $6\bar{\tau} < \tau < 20\bar{\tau}$, the mean and standard deviation of the cell swimming speed decrease linearly as τ increases. This suggests that by fitting a straight line and extrapolating back to $\tau = 0$ it is possible to estimate the true values. For smaller values of τ between $\bar{\tau}/2$ and $6\bar{\tau}$, the actual data are influenced by pixel noise and take higher values than would otherwise be expected.

7.3. $\tau \gg \bar{\tau}$

Consider first the case in which a cell has no preferred direction of travel and follows a correlated random walk with no bias. As $\tau \to \infty$, the rediscretized walk becomes wholly uncorrelated and

the p.d.f.'s of both the absolute angle, $f_\Theta(\theta)$, and the turning angle, $f_\Delta(\delta)$, become uniform so that all information about the correlation in the random walk is lost and the angular deviation of the turning angle, s_δ, tends to ∞ as τ tends to 0. Bovet & Benhamou (1988) have shown in practice that if the angular deviation $s_\delta \geqslant 1.2$ radians then it is not possible to reconstruct the random walk.

Secondly, if the random walk is biased, then when $\tau \to \infty$ the smoothing of the trajectories results in each segment of the trajectory being oriented towards the preferred direction, $\theta = \mu$, and the turning angles being zero so that

$$f_\Theta(\theta) \to \delta_D(\mu) \quad \text{and} \quad f_\Delta(\delta) \to \delta_D(0),$$

where δ_D is Dirac's delta function, so that

$$s_\delta \to 1 \quad \text{as} \quad \tau \to \infty.$$

Again, however, all information on $f_\Delta(\delta)$ is lost when the time step is very large.

7.4. CONSTRAINTS ON $\bar{\tau}$

Consideration of the cases when τ is large shows that a restriction on the data is that $\bar{\tau}$ should be sufficiently small that it is possible to extrapolate back to $\tau = 0$ in the original walk, i.e. $\bar{\tau}$ should be smaller than some critical value τ_c. Using numerical simulations, Bovet & Benham (1988) showed that, for an unbiased random walk, τ_c is such that the angular deviation of the turning angle s_δ should be less than 1.2 radians. Values of τ_c for biased correlated random walks await detailed numerical simulations which include pixel noise. Ideally, for the purposes of this paper, it should be shown that the criterion for the derivation of the Fokker–Planck equation, namely that $\sigma_\delta^2 \propto \tau$, is met, but the quality of the data is not good enough to confirm this.

7.5. HELICAL TRAJECTORIES

Most swimming cells rotate as they swim and asymmetries in their body shapes tend to cause them to travel along helical trajectories. Plots of trajectories, such as those in Fig. 1 for *C. nivalis*, suggest that the pitch and radius vary greatly across the populations that are analysed herein. The apparent helicity is smoothed out when the data are rediscretized over long time steps but this effect is difficult to quantify because of the variation across the population of cells. We are primarily interested in their velocity along the axis of the helices in the applications of our analysis and so, in calculating swimming speeds, we shall attempt to extrapolate back from the longer time-step discretizations. In calculating turning angles, we average over many

trajectories so that helicity will not affect the mean turning angles but will increase estimates of the angular deviation, σ_δ, making this a difficult quantity to measure.

8. Projection

The trajectories that are recorded by the image processor are projections, on to a two-dimensional plane, of individual cells swimming in three dimensions. However, since the suspension is viewed through a conventional microscope of small focal depth, cells moving outside the focal layer are not seen at all. In addition the cuvette is thin, being only 0.17 mm deep, which is of the order of 10 cell body lengths, so that the cells' motion is somewhat constrained to be planar. This raises the question of whether the recorded data should be analysed as being from a thin cross-section with little or no projection, or whether some allowance should be made for projection. This can be answered by testing the statistics of the apparent speed for data that is unimodal and axisymmetric, as follows.

Imagine as an extreme case that the microscope has infinite focal depth and that all the data from the swimming cells are full projections onto a vertical plane of their unconstrained three-dimensional trajectories. Suppose too that the cells' motion is symmetric about the vertical axis, and that the swimming speed, U say, is constant and thus independent of the direction. We want to know what the effect of the projection is on the statistics of the two-dimensional data that are recorded. Define fixed rectangular Cartesian axes $Oxyz$ with the z-axis vertically up and the x-axis lying in the plane of projection Oxz. The cells' direction in three dimensions is specified by spherical polar angles α and ϕ, where the colatitude α $(0 < \alpha < \pi)$ is measured from the negative y-axis (which is the axis of projection) and the meridional angle ϕ $(-\pi \leqslant \phi < \pi)$ is measured from the z-axis. This is a convenient choice of coordinates for analysis of the statistics of the projection. The Fisher distribution is a typical unimodal axisymmetric distribution on a sphere, analogous to the von Mises distribution on a circle, and has a p.d.f. given by

$$f_F(\alpha, \phi; \kappa) \, d\alpha \, d\phi$$

$$= \frac{\kappa}{4\pi \sinh \kappa} \exp(\kappa \sin \alpha \cos \phi) \sin \alpha \, d\alpha \, d\phi$$

where κ is the concentration parameter. This distribution is concentrated along the positive z-axis and is axisymmetric about Oz (Mardia, 1972; Fisher et al., 1987).

In the plane of projection, we define polar coordinates (r, θ) $(r \geqslant 0, -\pi \leqslant \theta < \pi)$ by

$$r = \sin \alpha, \quad \theta = \phi$$

so that $\theta = 0$ is the Oz-axis. The mapping from (α, ϕ) to (r, θ) is 1:1 for each hemisphere on either side of the plane of projection, Oxz. It follows that the p.d.f. of the Fisher distribution projected on to the plane, $f_P(r, \theta; \kappa)$, is given by

$$f_P(r, \theta; \kappa) \, dr \, d\theta$$

$$= \frac{\kappa}{2\pi \sinh \kappa} \exp(\kappa r \cos \theta) \frac{r}{\sqrt{1 - r^2}} \, dr \, d\theta,$$

from which it is straight forward to compute the conditional expectation of r, given a value of θ, to be

$$E(r|\theta; \kappa) = \int_0^1 \exp(\kappa r \cos \theta) \frac{r^2}{\sqrt{1 - r^2}} \, dr$$

$$\bigg/ \int_0^1 \exp(\kappa r \cos \theta) \frac{r}{\sqrt{1 - r^2}} \, dr.$$

In this example, the cells' swimming speed in three dimensions is a vector of length U so that the mean speed in the plane of projection is $\bar{v}(\theta) = UE(r|\theta; \kappa)$. $E(r|\theta; \kappa)$ is plotted in Fig. 3 for two values of the concentration parameter, $\kappa = 0.5, 2.0$. This shows clearly that when the swimming speed is independent of direction and when there is a bias towards swimming in the positive z-direction, then the average projected speed is greatest in the positive z-direction and least in the negative z-direction. Thus (as we shall
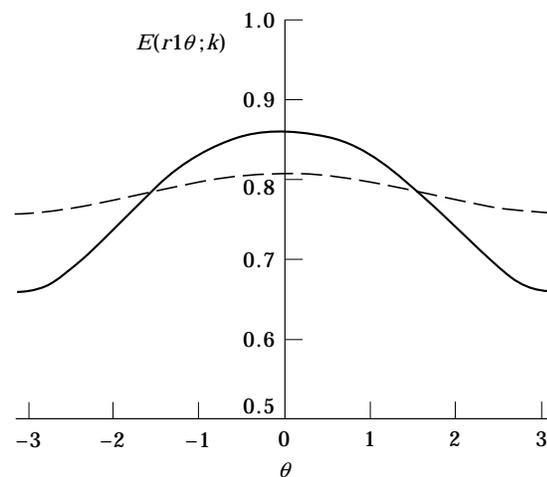

FIG. 3. Effect of projection on the mean value of the apparent speed, $E(r|\theta; \kappa)$, in the plane of projection, showing the dependence on θ for $\kappa = 0.5$ (dashed line) and 2.0 (solid line), when the true speed is one.

show) the absence of the same behaviour in our experimental data indicates that the effects of projection are not significant. Indeed, $\kappa = 0.5$ is a typical value for trajectories in these experiments, so that the difference between the minimum and maximum values of $\bar{v}(\theta)$ is only 6%, which is small compared with the scatter in the data.

9. Gravitaxis and Phototaxis

The motile algal cells that are mainly studied in this paper are *Chlamydomonas nivalis*. They are unicellular with a slightly prolate, spheroidal body about $10\,\mu$m in diameter and they swim using a pair of flagella approximately $10\,\mu$m in length, which they beat in a breast-stroke-like fashion, albeit at low Reynolds numbers, with a frequency of about 60 Hz. As is shown below, they swim at speeds of about four body lengths per second. The other alga studied is the dinoflagellate *Peridinium gatunense*. It is almost spherical in shape with a diameter of about $30\,\mu$m and is covered by rigid armoured plates. It swims using two heterodynamic flagella. One flagellum projects backwards from a longitudinal groove. A wave is passed along this flagellum in order to propel the cell forward. The second flagellum is ribbon-like and is located in a transverse groove. Waves are also passed along this flagellum, which appears to control the rotation of the cell about its longitudinal axis. Like most dinoflagellates, *P. gatunense* is a very active swimmer. Both of these species of cells are known to have at least two mechanisms for orientation, gravitaxis and phototaxis.

The first mechanism, strictly negative gravitaxis, orients the cells so that they swim upwards on average and is believed to be caused by a passive, mechanical torque due to the cells being bottom-heavy (Kessler, 1986). This is not the case for another common alga, *Euglena gracilis*. which has been shown to have an active gravitational orientation mechanism (Lebert & Häder, 1996) that depends on small strains in the cell membrane, which are due to the cell contents being about 4% denser than the fluid in which they swim, activating ion channels. Unlike *Euglena*, which can also move along surfaces by actively deforming its membrane, *Chlamydomonas* appears to have a relatively rigid cell wall and an asymmetric distribution of mass.

Kessler was the first to discover this mechanism's role in the spontaneous generation of macroscopic bioconvection patterns and to study the phenomenon in detail. He shows that the rate of reorientation of a spherical cell, when it is not swimming vertically, is determined by the balance between the gravitational torque, due to its offset centre of mass, and the viscous torque as it rotates in the fluid, giving

$$\omega = \mathrm{d}\theta/\mathrm{d}t = -B^{-1}\sin\theta, \qquad (37)$$

where B is a constant that represents the typical reorientation time. The orientation due to the balance between viscous and gravitational torques is known as gyrotaxis. In contrast, phototaxis is an active internal mechanism by which the cells either swim towards the light, presumably to increase their rate of photosynthesis, or away from the light if it is too bright. Hill & Vincent (1993) and the references cited therein discuss possible strategies that the cells employ in phototaxis. When a light source above them is sufficiently bright, phototaxis dominates gravitaxis and cells will swim vertically downwards away from the source.

Casual observation through a microscope, however, reveals that the cells' motion is not deterministic. Variations in the direction and speed of motion are of several types: (i) the population of cells is not cloned so there are intrinsic differences in shape and behaviour between individual cells; (ii) the internal biochemistry of individual cells is such that they capriciously change their velocity and occasionally do not swim at all; and (iii) cells collide with one another and with the walls of the container, which introduces further randomness into cell trajectories (Kessler *et al.*, 1992). Experiments have shown that this last effect becomes significant at cell concentrations greater than about 5×10^6 cells cm^{-3}, which is higher than the cell concentrations used here. The stochastic nature of the cells' swimming means that eqn (37) describes the mean rate of reorientation in gravitaxis (without phototaxis) i.e.

$$E[\mathrm{d}\theta/\mathrm{d}t] = -B^{-1}\sin\theta, \qquad (38)$$

which implies that the mean turning angle defined in (21) is given by

$$E[\delta] \equiv \mu_\delta = -B^{-1}\tau\sin\theta \quad \text{as} \quad \tau \to 0. \qquad (39)$$

This is consistent with the derivation of the Fokker–Planck equation. Equation (39), of course, motivated the analysis of the sinusoidal reorientation model in Section 6.

The cell trajectories that we measure for gravitaxis are viewed in a vertical plane and we assume that the distributions are symmetric about the vertical axis. We seek to show that (39) is satisfied, to derive values for B and also for the angular deviation for the turning angle $\sigma_\delta^2(\theta)$. On the other hand, for phototaxis, data are collected from cells viewed in a horizontal plane and illuminated from the side but we have no prior model to suggest what form $\mu_\delta(\theta)$ and

TABLE 1
Table of data sets

Data set	Description
C1	*C. nivalis* recorded in a vertical plane guided by negative gravitaxis. The swimming behaviour is axisymmetric about the vertical axis.
C2	*C. nivalis* recorded in a horizontal plane. There is no preferred direction so the motion is axisymmetric.
C3	*C. nivalis* recorded in a horizontal plane subject to illumination of 80 klux from the side, resulting in positive phototaxis.
C4	*C. nivalis* recorded in a horizontal plane subject to illumination of 200 klux from the side, resulting in positive phototaxis.
P1	*P. gatunense* recorded in a horizontal plane. There is no preferred direction so the motion is axisymmetric.
P2	*P. gatunense* recorded in a vertical plane guided by negative gravitaxis. The swimming behaviour is axisymmetric about the vertical axis.

$\sigma_\delta^2(\theta)$ should take, although the limits (21) and (22) should still hold for the Fokker–Planck equation to be valid. We also seek information on the p.d.f.'s of the cells' swimming speeds in both cases to be able to complete the calculations of the bulk mean swimming velocity and cell diffusivity needed in continuum equations that describe the motion of the suspension of cells in bioconvection.

10. Swimming Speed Results

Data from six sets of experiments are presented in this section. The data sets are summarized in Table 1.

10.1. DATA SET C1 *C. nivalis*: GRAVITAXIS

In Fig. 4, we show the swimming speed statistics, as a function of the timestep τ used to analyse the data, for a combined data set consisting of some 700 trajectories of various lengths taken in three experiments over a period of approximately 40 minutes from the same algal culture. The original mean time step for this data was $\bar\tau = 0.08$ s. The measured speed is the apparent speed, not velocity, projected on to the vertical two-dimensional plane of view. Figure 4(a) is a histogram of the distribution of observed swimming speeds for values of τ equal to 0.1 s, 0.2 s and 0.3 s. These graphs show distributions, similar in shape to an exponential distribution ($f(x; \lambda) = x \exp(-\lambda x)$, $x \geqslant 0$), with a broad peak centred around 40 μm s^{-1}. The dependence of the mean speed, $\bar v$, and standard deviation, v_{sd}, on τ are shown in Fig. 4(b) and (c): in both cases there is a gradual decrease as τ increases.

Interpretation

Closer inspection reveals that both quantities decrease rapidly as τ increases for values of τ less than 0.6 s, and then decrease almost linearly for values of τ between 0.6 s and 3.0 s. As discussed in Section 7, the initial nonlinear decrease in $\bar v$ and v_{sd} is believed to be mainly due to smoothing of the artificial pixel noise introduced by the discretization of the video images, superimposed on the smoothing of the true trajectories over time steps greater than the correlation time. The subsequent linear decrease is seen for all the data sets whether or not there is a preferred direction of motion and probably arises from further smoothing of helical trajectories, as discussed in Section 7.5. For values of $\tau > 3.0$ s, the number of segments of trajectories becomes so few that the statistics are noisy and no general trend is discernable. In the absence of any more-detailed theory for the effects of smoothing and because data on the axial component of the motion of the cells along their helical trajectories is required in applications, the dashed straight lines in Fig. 4(b) and (c) have been fitted by linear regression to the data points for values of τ between 0.6 s and 3.0 s. Extrapolating back to $\tau = 0$ gives estimates of 55 μm s^{-1} and 31 μm s^{-1} for the true mean speed and its standard deviation, respectively.

To examine the possible effects of projection (see Section 8), the speed is plotted as a function of the angle θ to the vertical in Fig. 4(d). ($\theta = 0°$ is upwards.) The data are divided into 12 bins of 30° width and the mean value of the speed in each bin is plotted against the mid-point of the bin. Results are shown for a typical value of the timestep, 1.6 s, corresponding to the linear region of Fig. 4(b), and show little dependence on θ given the obvious noise in the data. There is no correspondence with the effects of projection suggested by Fig. 3, and so we conclude that projection is unimportant to within experimental errors because of the small focal depth of the microscope and because the cuvette is very thin.

10.2. DATA SET C2 *C. nivalis*: HORIZONTAL

C2 is a small data set consisting of about 70 trajectories of *C. nivalis* cells from a different culture to those in C1 above and experimented on on a different day. The cells were viewed in a horizontal plane swimming under the influence of negative gravitaxis alone, and there is no preferred direction of motion. The swimming speed statistics are shown in Fig. 5 and the same trends are seen as in Fig. 4 for the data set C1. In particular, we can extrapolate back from the linear regions of the graphs in Fig. 5(b) and (c), as

indicated by the dashed lines, to get $\bar{v} = 67\,\mu\mathrm{m\,s}^{-1}$ and $v_{sd} = 29\,\mu\mathrm{m\,s}^{-1}$ for the true mean speed and standard deviation, respectively. The value of $\bar{v}$ is 25% greater than for C1, presumably reflecting the difference in the ages of the cultures, although little is known in detail about how age affects swimming behaviour.

10.3. DATA SETS C3 AND C4 *C. nivalis*: PHOTOTAXIS

Figure 6 shows the speed statistics for data set C3, which contains approximately 1000 trajectories from three experiments taken over a period of about 15 minutes. The *C. nivalis* cells were viewed in a horizontal plane and subject to illumination of 80 klux from the side, which is sufficient to induce positive phototaxis (i.e. movement towards the source) and acts together with negative gravitaxis,

although the cells' motion is constrained by the shallow cuvette. The histogram of speeds in Fig. 6(a) shows a larger proportion of slow cells than the previous data set, and the mean speed and its standard deviation are plotted as functions of the time step τ in Fig. 6(b) and (c). Both $\bar{v}$ and v_{sd} decrease as τ increases due to smoothing of the trajectories by discretization.

Data set C4 consists of about 900 trajectories from two experiments taken over 15 minutes. The cells were again observed in a horizontal focal plane and were subject to illumination from the side, this time of 200 klux, which induces a more precise, positive phototactic response than in data set C3. The speed statistics are plotted in Fig. 7 and Fig. 7(a) shows that an even higher proportion of the population of cells is slow moving at small values of τ than in Fig. 6(a).
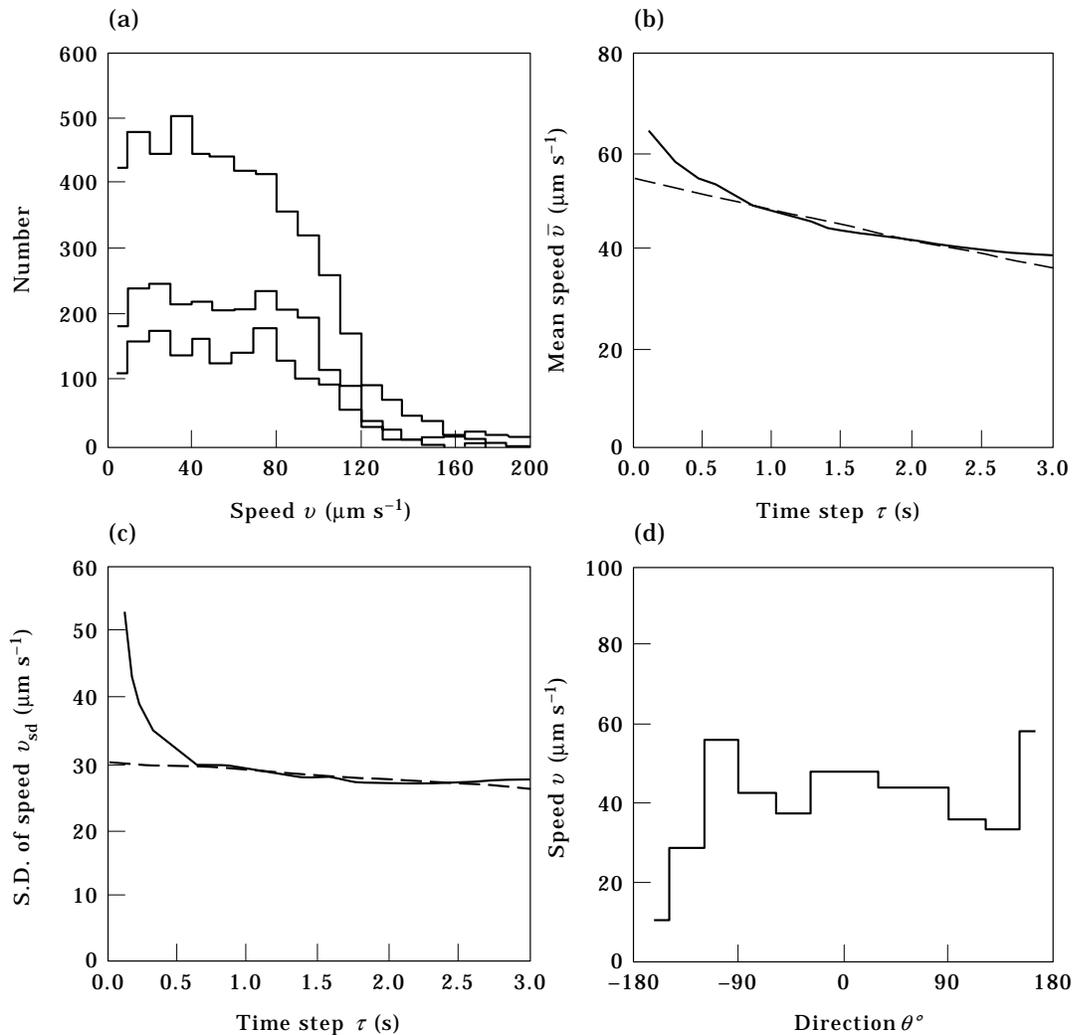

FIG. 4. Swimming speed statistics for data set C1, *C. nivalis* cells seen in a vertical plane. (a) Histograms of apparent swimming speeds, which decrease as the time step τ increases, for $\tau = 0.1$, 0.2 and 0.3 s. (b) and (c) Plots of the mean swimming speed and standard deviation (solid lines) vs. τ. The dashed lines are linear fits to the data for $0.6\,\mathrm{s} \leqslant \tau < 3.0\,\mathrm{s}$. (d) Histogram of swimming speed, v, vs. direction, θ, when $\tau = 1.6$ s, showing that v is independent of θ.

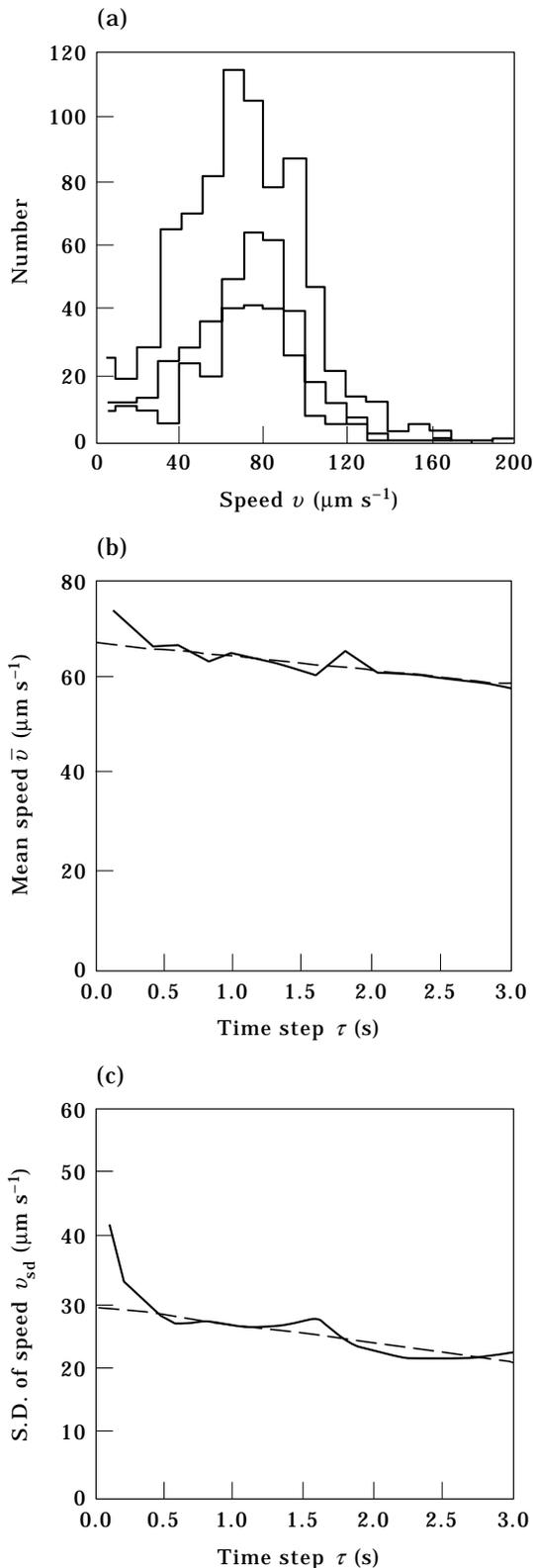**(a)**

(b)

(c)

FIG. 5. Swimming speed statistics for data set C2, *C. nivalis* cells seen in a horizontal plane. (a) Histograms of apparent swimming speeds, which decrease as the time step τ increases, for $\tau = 0.1$, 0.2 and 0.3 s. (b) and (c) Plots of the mean swimming speed and standard deviation (solid lines) vs. τ. The dashed lines are linear fits to the data for $0.6\,\mathrm{s} \leqslant \tau < 3.0\,\mathrm{s}$.

Figure 7(b) and (c) again shows that the mean speed and its standard deviation decrease as τ increases.

Interpretation

As described in Section 10.1, straight lines have been fitted to each of Figs 6(b), 6(c), 7(b) and 7(c). Extrapolating back to $\tau = 0$ gives $\bar{v} = 60\ \mu\mathrm{m\ s^{-1}}$ and $v_{sd} = 41\ \mu\mathrm{m\ s^{-1}}$ for the weaker illumination of 80 klux and $\bar{v} = 59\ \mu\mathrm{m\ s^{-1}}$ and $v_{sd} = 47\ \mu\mathrm{m\ s^{-1}}$ when the irradiance was 200 klux. The rather high value of v_{sd} in the latter case reflects the large number of slow cells.

In Fig. 6(d), the swimming speed for data set C3 when $\tau = 1.0$ s is plotted against θ, now the polar angle in the horizontal plane. $\theta = 0°$ is the direction towards the light, which is the preferred swimming direction as will be shown in Section 11.3. The graph indicates that the cells' swimming speed is in the main independent of the direction of motion, although there is an apparent decrease in swimming speed for values of θ between 90° and 180°.

In Fig. 7(d), we plot the swimming speed versus the polar angle θ in the horizontal plane when $\tau = 1.6$ s for data set C4. Again $\theta = 0°$ is the preferred direction and there is evidence that the swimming speeds away from the light are as little as 25% of those towards the light when $\tau = 1.0$ s. This suggests that *C. nivalis* exhibit a directed photokinetic response, namely their swimming speed depends on their direction of motion relative to the light source.

10.4. DATA SET P1 *P. gatunense*: HORIZONTAL

Approximately 1600 trajectories of *P. gatunense* cells seen in a horizontal plane from three experiments conducted over 30 minutes were recorded in data set P1. The speed statistics are shown in Fig. 8. The overall distribution of speeds in Fig. 8(a) is well peaked and we notice immediately that the mean speed is 2.5 to 3 times greater than that of *C. nivalis*. Consequently the number of data points per trajectory is smaller than for previous data sets because the time between points is determined by the cycle time of the computer algorithm, and also individual cells are more easily lost and reach the edges of the viewing area more rapidly. The distances between data points are greater too and so the effects of "pixel noise" are much reduced, as is evident in Fig. 8(b), which is approximately linear over the whole range of the timestep τ shown. Extrapolation gives the true mean speed to be $\bar{v} = 139\ \mu\mathrm{m\ s^{-1}}$. The graph of the standard deviation in Fig. 8(c) is irregular but, in order to make some estimate of the true value, a straight line was fitted by the method of least squares to the data points for values of τ between

0.6 s and 3.0 s. Extrapolation back to $\tau = 0$ s gives $v_{sd} = 46 \ \mu\text{m s}^{-1}$. The swimming speed is found to be independent of the direction of motion, as expected.

10.5. DATA SET P2 *P. gatunense*: GRAVITAXIS

The speed statistics for the data set P2 are shown in Fig. 9. About 700 trajectories were recorded from a different culture than that used in P1. The cells were recorded in a vertical plane swimming subject to negative gravitaxis. Again the distribution of speeds shown in Fig. 9(a) is strongly peaked. The graph of the mean speed, $\bar{v}$, in Fig. 9(b) is a little irregular and surprisingly takes values about a half of those for P1. On fitting the straight lines (drawn as dashed lines in the figures) by linear regression to the data points for values of τ between 0.6 s and 3.0 s, we estimate the true value of $\bar{v}$ to be 76 $\mu\text{m s}^{-1}$ with a correspondingly low standard deviation, $v_{sd} = 14 \ \mu\text{m s}^{-1}$. These differences between the speeds calculated for P1 and P2 may be due to the use of different cultures. As for *C. nivalis* subject only to negative gravitaxis, the mean speed in P2 is independent of the direction of swimming.

11. Angular Distribution Results

11.1. DATA SET C1 *C. nivalis*: GRAVITAXIS

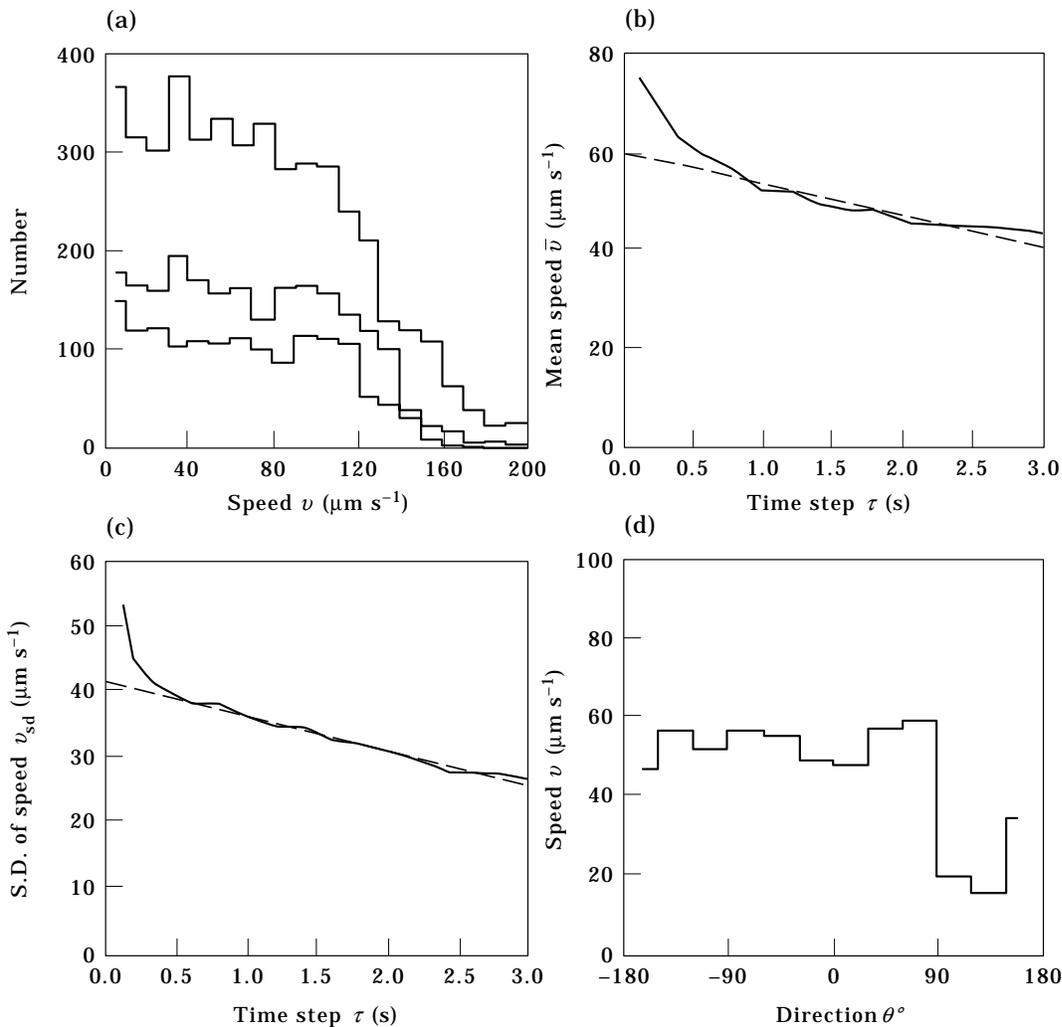As described in Section 9, *C. nivalis* cells are thought to be bottom heavy and subject to a

FIG. 6. Swimming speed statistics for data set C3, *C. nivalis* cells seen in a horizontal plane subject to 80 klux illumination from $\theta = 0°$. (a) Histograms of apparent swimming speeds, which decrease as the time step τ increases, for $\tau = 0.1$, 0.2 and 0.3 s. (b) and (c) Plots of the mean swimming speed and standard deviation (solid lines) vs. τ. The dashed lines are linear fits to the data for 0.6 s $\leqslant \tau < 3.0$ s. (d) Histogram of swimming speed, v, vs. direction, θ, when $\tau = 1.6$ s.
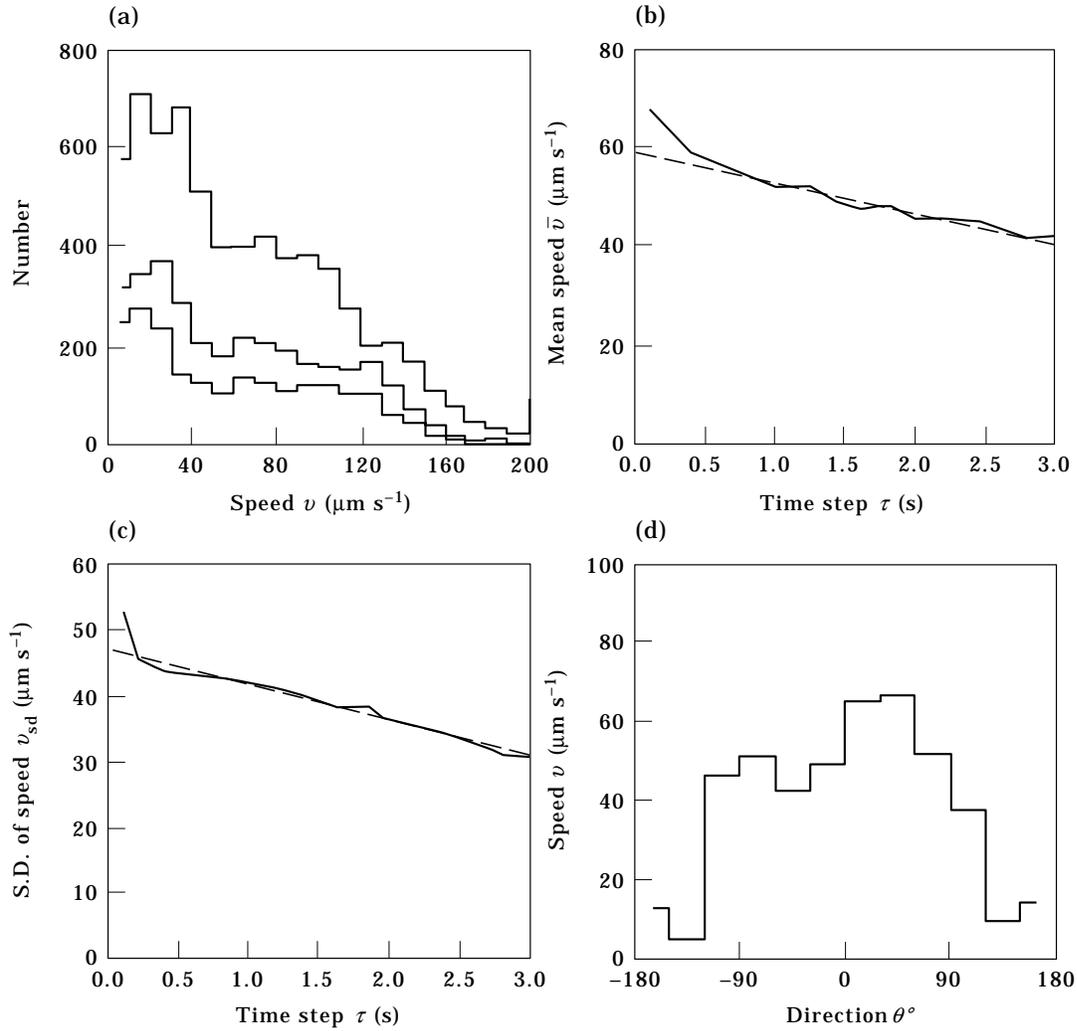
FIG. 7. Swimming speed statistics for data set C4, *C. nivalis* cells seen in a horizontal plane subject to 200 klux illumination from $\theta = 0°$. (a) Histograms of apparent swimming speeds, which decrease as the time step τ increases, for $\tau = 0.1$, 0.2 and 0.3 s. (b) and (c) Plots of the mean swimming speed and standard deviation (solid lines) vs. τ. The dashed lines are linear fits to the data for 0.6 s $\leqslant \tau < 3.0$ s. (d) Histogram of swimming speed, v, vs. direction, θ, when $\tau = 1.6$ s, showing evidence that the speed towards the source is greater than away from it (photokinesis).

passive gravitational torque orients them so that they swim vertically up on average. In Fig. 10, we show graphs of the mean turning angle, μ_δ, as a function of the swimming direction θ, for increasing values of the timestep τ. $\theta = 0$ is vertically upwards. The turning angles have been averaged over 12 intervals of $30°$ width according to the swimming direction, θ and are represented by the solid lines that connect the midpoints of the bins. The numbers of data points for each bin are shown in Table 2. We see that μ_δ tends to be positive when θ is negative and vice versa, and that μ_δ increases with τ. These observations are consistent with the cells swimming upwards on average because the signs of the mean turning angles

are such as to correct deviations from the vertical. They also show that changes in direction decrease as τ decreases i.e. that the motion is correlated and changes in direction are gradual.

Interpretation

Curves of the form

$$\mu_\delta = -d(\tau)\sin \theta, \tag{40}$$

where $d(\tau)$ is a parameter representing the "turning amplitude" [see eqn (37)], have been fitted using the method of least squares to each of the curves in Fig. 10 and are shown as dashed lines. The fit is
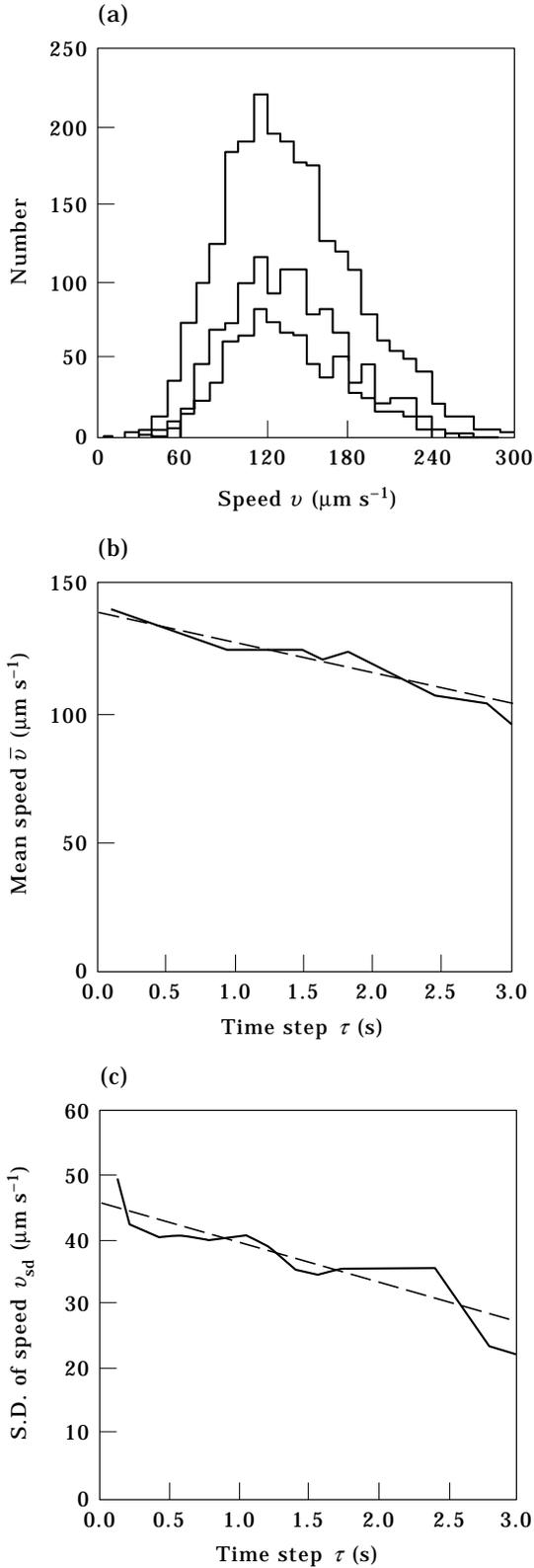
FIG. 8. Swimming speed statistics for data set P1, *P. gatunense* cells seen in a horizontal plane. (a) Histograms of apparent swimming speeds, which decrease as the time step τ increases, for $\tau = 0.1, 0.2$ and 0.3 s. (b) and (c) Plots of the mean swimming speed and standard deviation (solid lines) vs. τ. The dashed lines are linear fits to the data for 0.6 s $\leqslant \tau < 3.0$ s.

reasonable, particularly for smaller values of $\tau \leqslant 0.4$ s for which the data are smoother. The estimates of the turning amplitude are plotted as a function of the time step, τ, and shown as the solid line in Fig. 11(a). There is some scatter in the data but clearly $d(\tau)$ increases with τ on average. The limits taken in the derivation of the Fokker–Planck equation [see eqns (21) and (22)] require that $\delta(\tau) \propto \tau$ but the data are too scattered to confirm or reject this hypothesis. Nevertheless, in order to make estimates of the coefficients in the Fokker–Planck equation, a straight line through the origin has been fitted by linear regression and is plotted as the dashed line in Fig. 11(a). The gradient of this line is $d_0 = 0.37$ rad s^{-1} from which we estimate that

$$\mu_\delta = \mu_0(\theta)\tau \quad \text{and} \quad \mu_0 = 0.37 \sin \theta,$$

where μ_0 is the orientation (or drift) coefficient in the Fokker–Planck equation (24). Also, from eqn (39), a typical cell reorientation time is

$$B = d_0^{-1} = 2.7 \text{ s}.$$

The possible error in estimating d_0 is relatively large due to the scatter in the data. It is also questionable whether or not the data points for $\tau \leqslant 0.4$ s are more reliable. A straight line fitted to these points, the dotted line in Fig. 11(a), gives an alternative estimate which is that $d_0 = 0.80$ and correspondingly $B = 1.25$ s.

The second quantity of interest is the angular deviation $\sigma_\delta(\theta, \tau)$ of the turning angle distribution, and graphs of these data as functions of θ for two values of τ are plotted in Fig. 11(b), using Definition (1). It is immediately clear that there is no obvious dependence on τ and that there may be a weak dependence on θ of the form

$$\sigma_\delta(\theta) = a - b \sin \theta,$$

where $a \approx 1.2$ rad and $b \approx 0.2$ rad, but the noise in the data renders it difficult to reliably estimate a, b and to test for dependence on τ. For mathematical modelling purposes, a good first approximation is to assume that $\sigma_\delta(\theta, \tau)$ is independent of θ, and so we choose to examine the behaviour of $\bar{\sigma}_\delta(\tau)$, the overbar indicating the mean value of $\sigma_\delta(\theta, \tau)$ averaged over all values of the swimming direction θ, which is graphed in Fig. 11(c). This shows that $\bar{\sigma}_\delta(\tau)$ increases as τ increases from 0.1 s to 0.4 s, reaching a maximum value of about 1.2 radians, and then gradually decreases as τ increases further. This behaviour is also found in numerical simulations of random walks (which are currently under investigation and will be reported in a separate paper later) and can be understood as follows.
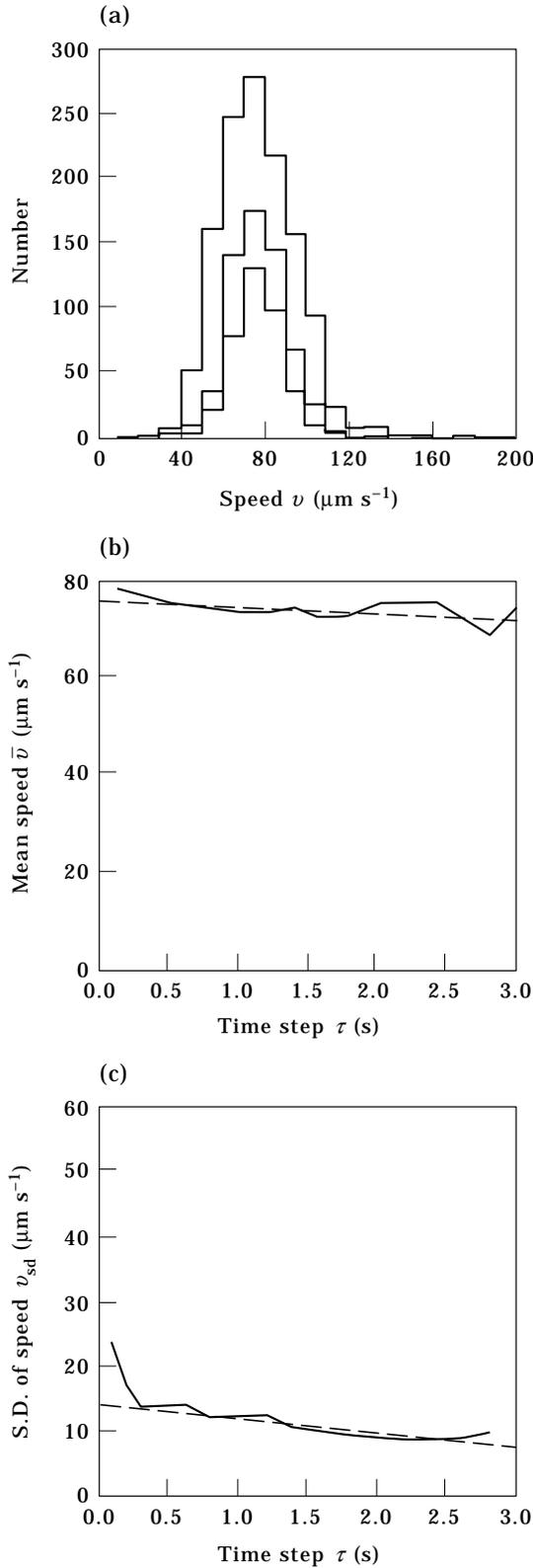
(a)

(b)

(c)

FIG. 9. Swimming speed statistics for data set P2, *P. gatunense* cells seen in a vertical plane. (a) Histograms of apparent swimming speeds, which decrease as the time step τ increases, for $\tau = 0.1, 0.2$ and 0.3 s. (b) and (c) Plots of the mean swimming speed and standard deviation (solid lines) versus τ. The dashed lines are linear fits to the data for $0.6 \text{ s} \leqslant \tau < 3.0 \text{ s}$.

Bovet & Benhamou (1988) demonstrated that for an unbiased, correlated random walk $\sigma_\delta(\tau) \propto \sqrt{\tau}$, so that measurements of the turning angle become less correlated as the time scale τ is increased. However, for a *biased* random walk, the segments of the trajectory become more likely to be aligned closely with the preferred direction as τ is increased and the segments become longer. Thus the p.d.f. of the swimming direction, θ, becomes more peaked about the preferred direction, μ_θ say, as τ increases, with a consequent reduction in the mean turning angle $\mu_\delta(\tau)$ and thus in $\sigma_\delta(\tau)$. Of course, the statistical analysis is complicated further by pixel noise for small values of τ, by the smoothing of helical trajectories, and by the decreasing number of data points for large values of τ, all of which augment the observed values of $\sigma_\delta(\tau)$.

As a consequence of these effects, it is not possible to reliably estimate the true limiting behaviour of $\sigma_\delta(\tau)$ as $\tau \to 0$. Fortunately, additional information can be gleaned from studying the p.d.f., $f(\theta)$, of the direction of swimming, which is plotted for a typical time step $\tau = 0.4$ s as the histogram in Fig. 11(d). From the estimates for the mean angle, $\mu\theta = 22°$, and the mean length, $r = 0.22$, for the swimming direction, θ, a von Mises p.d.f. has been fitted and is plotted as the solid line. The fit is good. The mean swimming direction, μ_θ, differs a little from the vertical which may be due to thermal convection currents in the cuvette during the experiments. This will also have contributed to the error in fitting the sinusoidal curves to $\mu_\delta(\theta)$ in Fig. 10. As expected, μ_θ proves to be independent of τ, and the plot of the angular deviation of θ, $\sigma_\theta(\tau)$, in Fig. 11(e) shows that it decreases linearly and very gradually with τ. Extrapolating back to $\tau = 0$, shows that $\sigma_\theta(0)$ lies between 1.7 and 1.9 radians. The very weak dependence of σ_θ on τ permits the calculation of an estimate of $\sigma_\delta(\tau)$ from d_0 and σ_θ from eqn (31), using the analysis of the sinusoidal reorientation model of Section 6.

For this data set, we have estimated that $d_0 = 0.37$ rad (or 0.80 rad) and $\sigma_\theta = 1.8 \pm 0.1$ rad, which implies that the best estimate for the angular deviation of δ is

$$\sigma_\delta = 1.3\sqrt{\tau} \quad \text{or} \quad 2.0\sqrt{\tau} \text{ rad.}$$

Using eqn (25), this gives the effective rotational diffusivity to be

$$D = 0.85 \quad \text{or} \quad 2.0 \text{ rad}^2 \text{ s}^{-1}.$$

As well as the actual estimates of parameters, the key points from the above statistical analysis are:
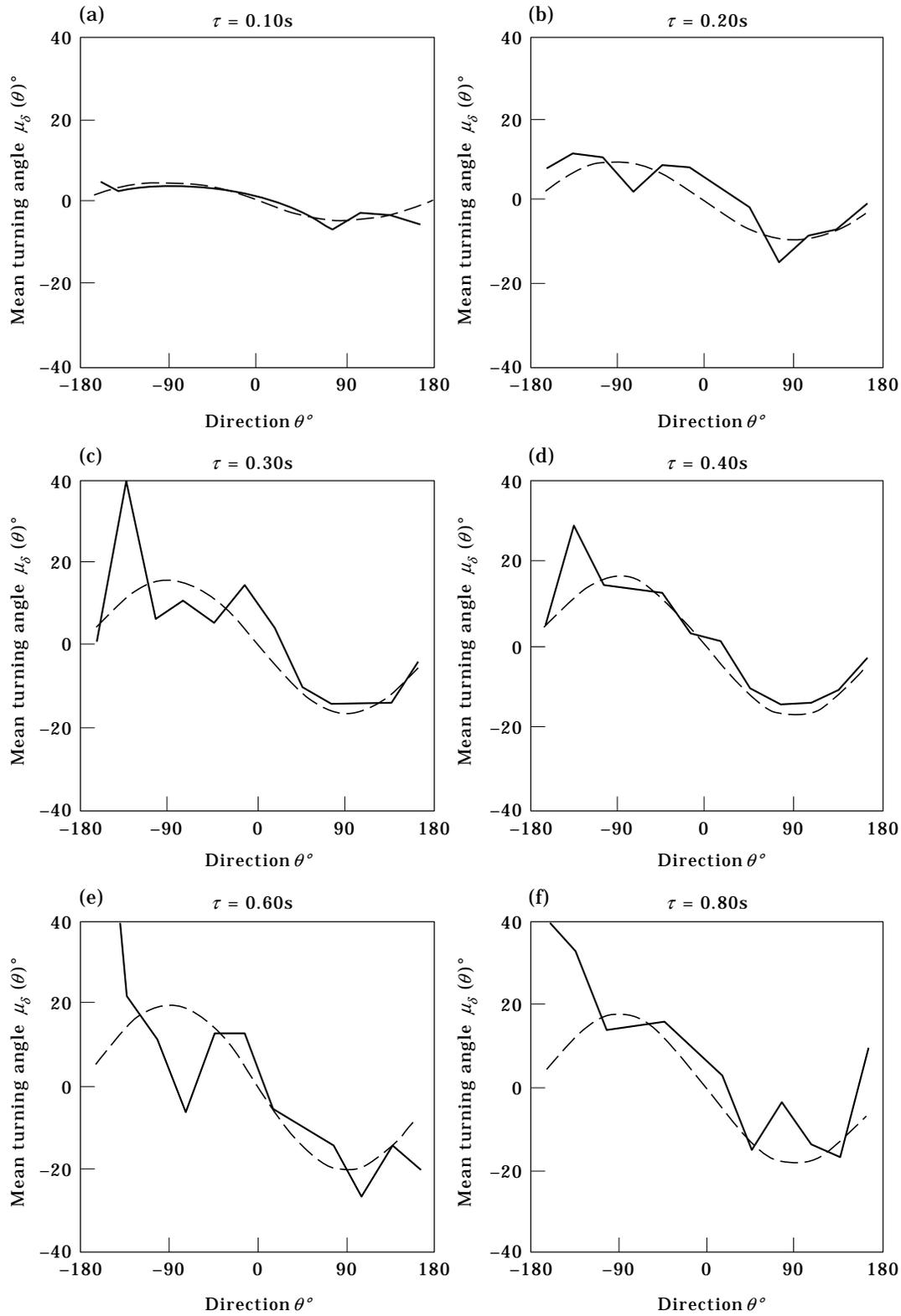
FIG. 10. Angular statistics for data set C1, *C. nivalis* cells seen in a vertical plane. Graphs of the mean turning angle, μ_δ, vs. the swimming direction, θ, (solid lines) are shown for successive values of the time step, τ. Curves of the form $-d(\tau)\sin\theta$ (dashed lines) have been fitted to the data using the method of least squares.

TABLE 2

Numbers of data points for calculating the mean turning angle, μ_δ, for data set C1 as a function of the swimming direction, θ, and the time step, τ

Time step	Swimming direction $\theta°$											
$\tau(s)$	-165	-135	-105	-75	-45	-15	15	45	75	105	135	165
0.1	400	364	654	540	595	427	467	354	234	331	245	320
0.4	84	66	96	138	120	92	80	64	61	46	50	70
1.0	12	12	28	35	25	14	17	15	9	8	14	14
1.6	5	2	9	11	11	1	8	3	3	1	2	4

Note that the number of data points decreases as τ increases so that the statistics become less significant for larger time steps.

(1) the turning angle data support the conclusion that $\mu_\delta = -d_0\tau \sin\theta$, which validates the assumption of orientation due to a gravitational torque and is consistent with a description of the cells' motion as the continuous limit of a biased random walk;

(2) the independence of μ_θ on τ is as predicted by the solution of the Fokker–Planck equation derived from the random walk model.

11.2. DATA SET C2 *C. nivalis*: HORIZONTAL

Data set C2 is taken from *C. nivalis* cells viewed swimming in a horizontal plane. Gravitaxis, due to the cells being bottom heavy, is the only orientating mechanism in the absence of illumination, and so there should be no preferred direction of motion in the *horizontal* plane. Plots of the mean turning angle, $\mu_\delta(\theta)$, (not shown) confirm that $\mu_\delta(\theta)$ is independent of the swimming direction θ and that it is approximately zero, as expected. The graph of $\sigma_\delta(\tau)$ should show that $\sigma_\delta(\tau) \propto \sqrt{\tau}$ as described by Bovet & Benhamou (1988) but the data are noisy and no clear trend can be seen, probably because the data set is too small and consists of only 70 trajectories.

11.3. DATA SETS C3 AND C4 *C. nivalis*: PHOTOTAXIS, 80 KLUX AND 200 KLUX

The swimming cells, whose trajectories were recorded in data sets C3 and C4 in a horizontal plane, were subject to illumination from $\theta = 0°$, which induced positive phototaxis. Of course, the cells are also oriented by gravitaxis, so the overall preferred swimming direction will be at an angle between the upwards vertical and $\theta = 0°$ in the horizontal plane (Kessler *et al.* 1992), but again any vertical motion is constrained by the shallow cuvette. Plots of $\mu_\delta(\theta)$ are shown for the two data sets in Figs 12(a) and 13(a) for typical values of the time step. The solid lines are for $\tau = 0.3$ s and the dashed lines for $\tau = 0.6$ s. Unlike orientation by gravitaxis for which $\mu_\delta(\theta) \propto -\sin\theta$ as discussed in Section 10.1, it appears that $\mu_\delta(\theta) \propto -\theta$ for phototaxis, although the points at the ends of the graphs ($|\theta| \geqslant 165°$) become very

variable as τ increases due to there being very few longer segments of trajectories lying in these directions.

Interpretation

Straight lines of the form $\mu_\delta(\theta) = -d(\tau)\theta$ have been fitted by linear regression to the central points of the graphs ($|\theta| < 165°$), and graphs of $d(\tau)$ against τ are shown as the solid curves in Figs 12(b) and fitted to all the data by linear regression and is plotted as the dashed line. The fit is good and we estimate that

$$d = 0.44\tau$$

so that $\mu_\delta(\theta) = -0.44\tau$. The linear dependence on τ is consistent with the limits required in the derivation of the Fokker–Planck equation (24), and thus the coefficient $\mu_0(\theta)$ in the Fokker–Planck equation is estimated to be

$$\mu_0(\theta) = -0.44\theta.$$

As for data set C1 in Section 10.1, it may be that more reliable estimates would be derived from fitting a straight line to those data for which $\tau \leqslant 0.4$ s; such a fit is shown as the dotted line in Fig. 12(b), from which we calculate that $\mu_0(\theta) = -0.62\theta$.

There is rather more scatter in the values of $d(\tau)$ from data set C4 [Fig. 13(b)]. Again to estimate $\mu_0(\theta)$, straight lines have been fitted as described above and leads us to calculate, with some reservations, that

$$\mu_0(\theta) = -0.19\theta \quad \text{or} \quad -0.61\theta.$$

Plots of the angular deviation, $\sigma_\delta(\theta)$, for fixed values of τ are shown in Figs 12(c) and 13(c) for typical values of the time step. The solid lines are for $\tau = 0.3$ s and the dashed lines for $\tau = 0.6$ s. For both data sets, independently of τ, $\sigma_\delta(\theta)$ takes its largest values at the endpoints ($|\theta| > 135°$) corresponding to swimming directions away from the light source where there are fewer data points. For any given value of τ, $\sigma_\delta(\theta)$ is roughly constant for the central values of θ ($|\theta| < 135°$).

Graphs of the mean angular deviation, $\sigma_\delta(\tau)$, averaged over all values of the swimming direction θ
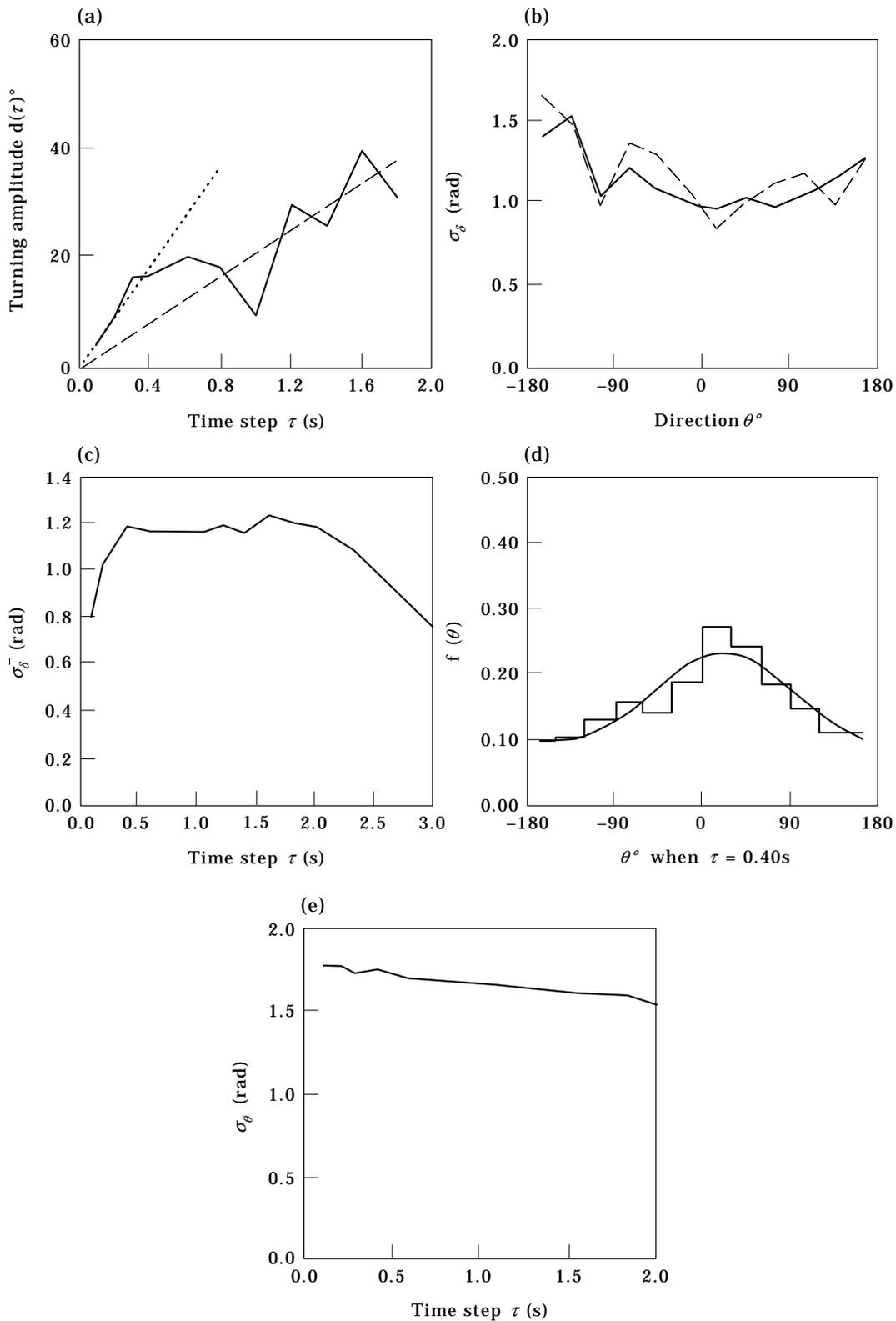
FIG. 11. Angular statistics for data set C1, *C. nivalis* cells seen in a vertical plane. (a) Plot of the turning amplitude, *d* vs. time step, τ. Straight lines through the origin have been fitted using linear regression to all the data (dashed line) and to the data for which $\tau \leqslant 0.4$ s (dotted line). (b) Graphs of the angular deviation of the turning angle, σ_δ, vs. swimming direction, θ, for $\tau = 0.3$ s (solid line) and for $\tau = 0.6$ s (dashed line). (c) Plot of the mean angular deviation of the turning angle, $\sigma_\delta(\tau)$, averaged over all swimming directions, vs. τ. (d) Histogram of the p.d.f., $f(\theta)$, of the swimming direction, θ, over which is plotted a von Mises p.d.f. that has been fitted using the mean angle and length for the θ-statistics. (e) Plot of the angular deviation, σ_θ, of the swimming direction showing linear dependence on τ.
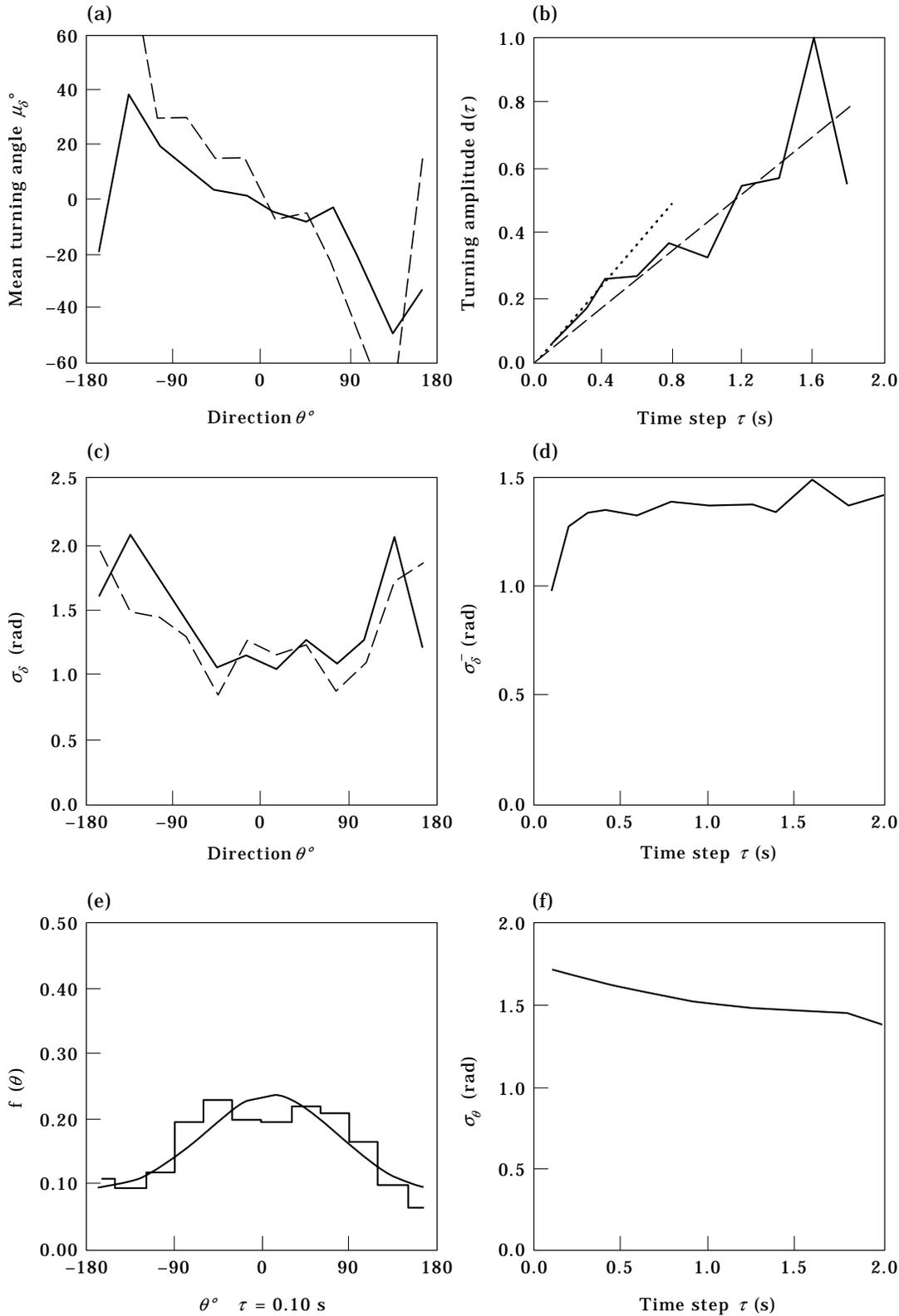
FIG. 12. Angular statistics for data set C3, *C. nivalis* cells seen in a horizontal plane subject to 80 klx illumination from $\theta = 0°$. (a) Graphs of the mean turning angle, μ_δ, vs. the swimming direction, θ, are shown for $\tau = 0.3$ s (solid line) and for $\tau = 0.6$ s (dashed line). Straight lines of the form $-d(\tau)\theta$ have been fitted to the data for which $|\theta| < 165°$, using the method of least squares. (b) Plot of the turning amplitude, d, vs. time step, τ. Straight lines through the origin have been fitted using linear regression to all the data (dashed line) and to the data for which $\tau \leqslant 0.4$ s (dotted line). (c) Graphs of the angular deviation of the turning angle, σ_δ, vs. swimming direction, θ, for $\tau = 0.3$ s (solid line) and for $\tau = 0.6$ s (dashed line). (d) Plot of the mean angular deviation of the turning angle, $\sigma_\delta(\tau)$, averaged over all swimming directions, vs. τ. (e) Histogram of the p.d.f., $f(\theta)$, of the swimming direction, θ, over which is plotted a von Mises p.d.f. that has been fitted using the mean angle and length for the θ-statistics. (f) Plot of the angular deviation, σ_θ, of the swimming direction.
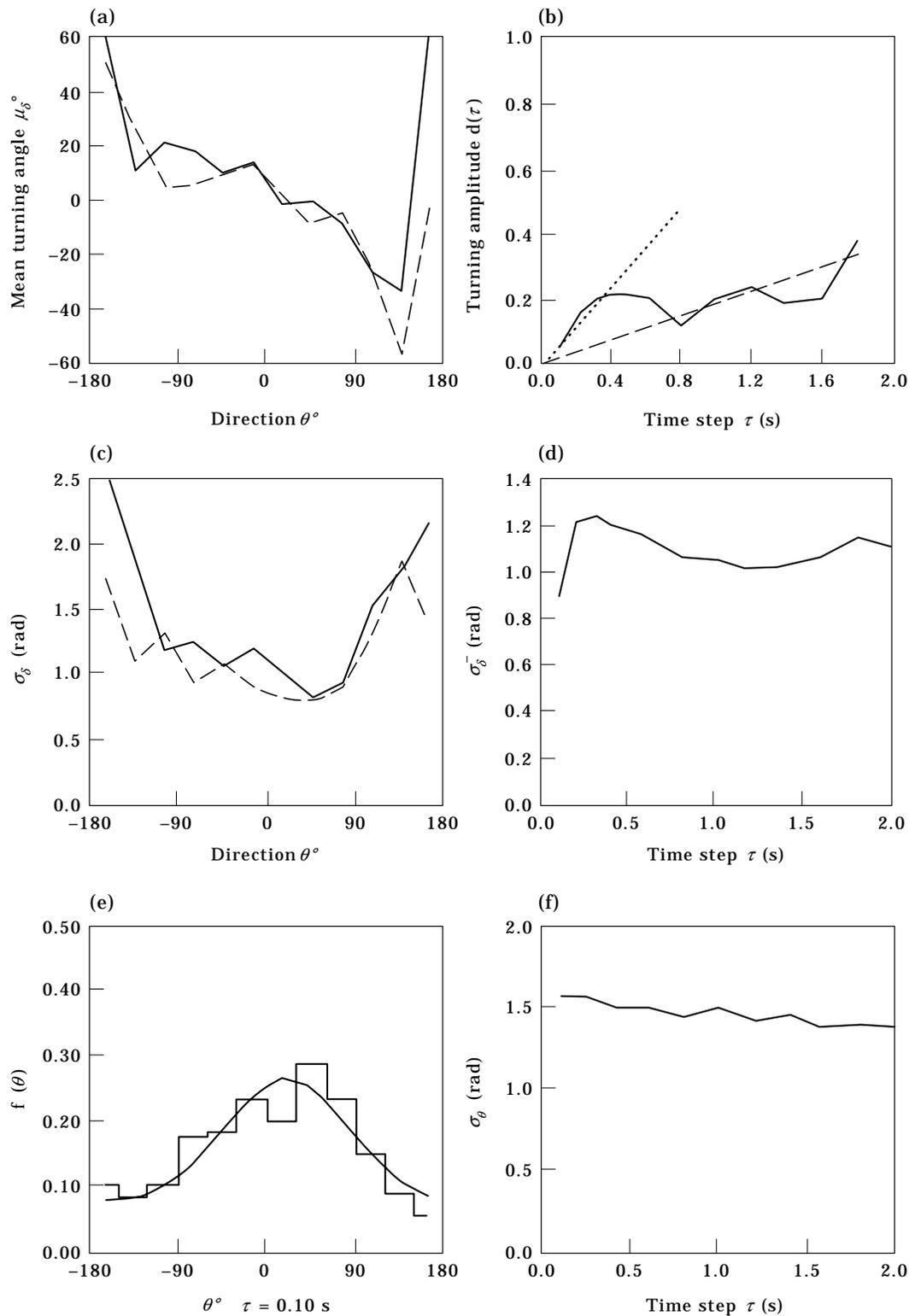
522

Fɪɢ. 13. Angular statistics for data set C4, *C. nivalis* cells seen in a horizontal plane subject to 200 klx illumination from $\theta = 0°$. (a) Graphs of the mean turning angle, μ_δ, vs. the swimming direction, θ, are shown for $\tau = 0.3$ s (solid line) and for $\tau = 0.6$ s (dashed line). Straight lines of the form $-d(\tau)\theta$ have been fitted to the data for which $|\theta| < 165°$, using the method of least squares. (b) Plot of the turning amplitude, d, vs. time step, τ. Straight lines through the origin have been fitted using linear regression to all the data (dashed line) and to the data for which $\tau \leqslant 0.4$ s (dotted line). (c) Graphs of the angular deviation of the turning angle, σ_δ, vs. swimming direction, θ, for $\tau = 0.3$ s (solid line) and for $\tau = 0.6$ s (dashed line). (d) Plot of the mean angular deviation of the turning angle, $\sigma_\delta(\tau)$, averaged over all swimming directions, vs. τ. (e) Histogram of the p.d.f., $f(\theta)$, of the swimming direction, θ, over which is plotted a von Mises p.d.f. that has been fitted using the mean angle and length for the θ-statistics. (f) Plot of the angular deviation, σ_θ, of the swimming direction.

are presented in Figs 12(d) and 13(d). These show similar behaviour as in the gravitactic case, C1, with a rapid increase with τ for values of $\tau \leqslant 0.4$ s and little dependence on τ for larger values of τ. In general for any given value of τ, $\sigma_\delta(\tau)$ is smaller for C4 than for C3.

The p.d.f.'s, $f(\theta)$, for swimming directions are shown as histograms in Figs 12(e) and 13(e) for $\tau = 0.1$ s. The solid curves show von Mises p.d.f.'s, $M(\theta; 0, \kappa)$, where

$$A(\kappa) = \exp(-\sigma_\theta^2(\tau)/2)$$

as in eqn (10) which have been fitted from the calculated values of the mean direction and mean angle for the Θ-statistics. The p.d.f.'s for all values of τ are unimodal and show little dependence on τ. Those for C3 have a fairly broad peak centred on $\theta = 0°$ towards the light source. The distribution for C4 is more sharply peaked because $\sigma_\delta(\tau)$ is smaller for C4 than for C3, even though the values of $\mu_0(\theta)$ are also smaller for C4 than for C3, showing that the brighter illumination elicits a stronger phototactic response. Graphs of the angular deviation for θ, $\sigma_\theta(\tau)$, versus τ, in Figs 12(f) and 13(f), show that $\sigma_\theta(\tau)$ decreases very linearly with τ, as is the case for data set C1, and linear interpolation gives $\sigma_\theta(0) = 1.7$–1.8 rad and 1.5–1.6 rad for C3 and C4 respectively.

As in the geotactic case 1, it is possible to estimate the limiting behaviour of $\sigma_\delta(\tau)$ from the values of $\sigma_\theta(0)$ and $\mu_0(\theta)$ by inverting equation (36) from the analysis for the linear orientation model in Section 6. For data set C3, we find that $\sigma_\delta(\tau) = 1.8\sqrt{\tau}$ radians

if we take $\mu_0(\theta) = -0.44\ \theta$, and $\sigma_\delta(\tau) = 2.1\sqrt{\tau}$ radians if $\mu_0(\theta) = -0.62\ \theta$. For C4, $\sigma_\delta(\tau) = 0.9\sqrt{\tau}$ radians if $\mu_0(\theta) = -0.19\ \theta$, and $\sigma_\delta(\tau) = 1.7\sqrt{\tau}$ radians if $\mu_0(\theta) = -0.61\ \theta$.

11.4. DATA SET P1 *P. gatunense*: HORIZONTAL

The *P. gatunense* cells in this data set were recorded swimming in a horizontal plane, so there is no preferred horizontal direction. A logarithmic graph of the angular deviation $\sigma_\delta(\tau)$ is plotted in Fig. 14(a). $\ln \sigma_\delta(\tau)$ appears to depend linearly on τ and thus the straight line

$$\ln \sigma_\delta(\tau) = m \ln \tau + \ln \sigma_0,$$

where m and σ_0 are parameters, has been fitted to the data for values of $\tau \leqslant 0.4$ s by the method of least squares and is plotted as the dashed line in the figure. The slope is $m = 0.43$, which is acceptably close to the value of 0.5 that would be expected if $\sigma_\delta(\tau) = \sigma_0\sqrt{\tau}$ as required when taking the limits (22) in the derivation of the Fokker–Planck equation. We also estimate that $\sigma_0 = 0.91$ rads$^{-1/2}$. This gives an upper bound on values of $\sigma_\delta(\tau)$ due to the additional contribution from the pixel noise. Analysis of the angular deviation, $\sigma_\theta(\tau)$ of the swimming direction in Fig. 14(b) shows once again that it gradually decreases linearly as τ increases and by extrapolation that $\sigma_\theta(0) = 1.8$–1.9 rad.

11.5. DATA SET P2 *P. gatunense*: GRAVITAXIS

Finally we note that there was too much scatter in the angular statistics of data set P2, for *P. gatunense*
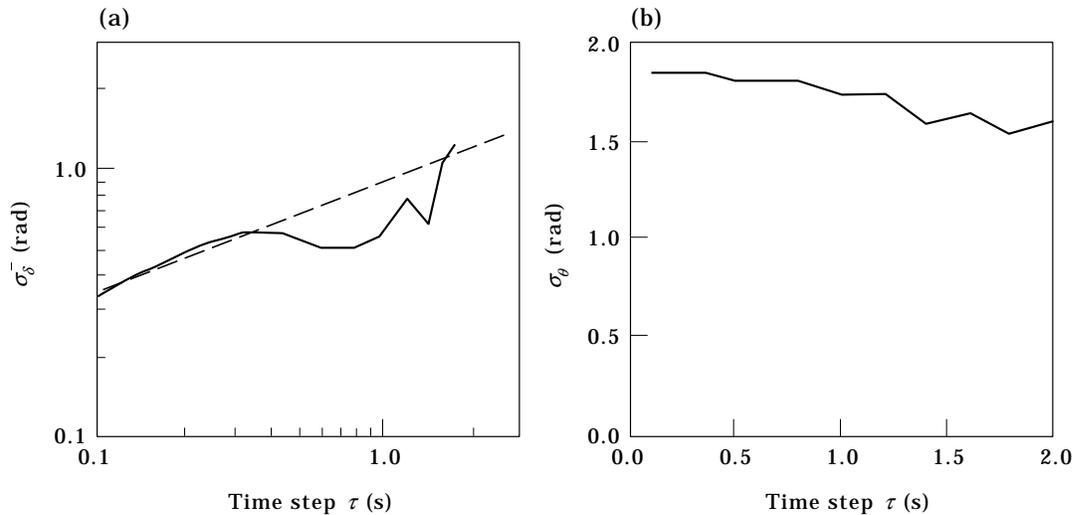

FIG. 14. Angular statistics for data set P1, *P. gatunense* cells seen in a horizontal plane. (a) Logarithmic plot of the mean angular deviation of the turning angle, $\sigma_\delta(\tau)$, averaged over all swimming directions (solid line), vs. τ. A straight line (dashed line) has been fitted to those data for which $\tau \leqslant 0.4$ s. (b) Plot of the angular deviation, σ_θ, of the swimming direction.

TABLE 3
Summary of results

Data set	C1 (vertical)	C2 (horizontal)	C3 (phototaxis: 80 klux)
$\bar{v}(\mu\text{m s}^{-1})$	55	67	60
$v_{sd}(\mu\text{m s}^{-1})$	31	29	41
$\mu_0(\theta)(\text{rad})$	$-0.37\,(0.80)\tau\sin\theta$	—	$-0.44\,(0.62)\theta$
$\sigma_\delta(\tau)(\text{rad})$	$1.3\,(2.0)\sqrt{\tau}$	—[1]	$1.8\,(2.1)\sqrt{\tau}$
$\sigma_\theta(\text{rad})$	1.8 ± 0.1	—[1]	1.75 ± 0.05
$D = \sigma_0^2/2(\text{rad}^2\,\text{s}^{-1})$	$0.85\,(2.0)$	—[1]	$1.6\,(2.2)$
Notes	$B = 2.7\,(1.3)$ s	[1] No data	

Data set	C4 (phototaxis: 200 klux)	P1 (horizontal)	P2 (vertical)
$v(\mu\text{m s}^{-1})$	59[2]	139	76
$v_{sd}(\mu\text{m s}^{-1})$	47[2]	46	14
$\mu_0(\theta)(\text{rad})$	$-0.19\,(0.61)\theta$	—	—[3]
$\sigma_\delta(\tau)(\text{rad})$	$0.9\,(1.7)\sqrt{\tau}$	$0.91\sqrt{\tau}$	—[3]
$\sigma_\theta(\text{rad})$	1.55 ± 0.05	1.85 ± 0.05	—[3]
$D = \sigma_0^2/2(\text{rad}^2\,\text{s}^{-1})$	$0.40\,(1.4)$	0.41	—[3]
Notes	[2] Photokinesis		[3] No data

$\bar{v}$ and v_{sd} are the mean swimming speed and its standard deviation
$\mu_0(\theta)$ is the oritation coefficient in the Fokker–Planck equation. $\sigma_\delta(\tau)$ and σ_θ are the angular deviations of the mean turning angle and swimming direction, respectively. D is the effective rotational diffusivity and B is the gyrotactic reorientation time. Numbers in parentheses are based on alternative estimates for the value of the mean turning angle when $\tau = 0$.

cells viewed in a vertical plane, to obtain significant turning angle statistics. This is surprising, given that data from over 700 trajectories were recorded, but plots of the trajectories show that most are very straight and show little evidence of turning, so this type of analysis may be inappropriate for these micro-organisms. This argument is supported by the observation that the p.d.f., $f(\theta)$, for the direction of swimming was seen to be sharply peaked at $0°$ (confirming that the cells are negatively gravitactic), but it is not well-fitted by a von Mises distribution because the central peak in the data is too narrow.

All the above results are summarized in Table 3.

12. Conclusions

A new theory for modelling the trajectories of motile algal cells that are swimming in a preferred direction has been presented. The model is based on the continuous limit of a biased, correlated, random walk as the time step tends to zero. It has been successfully tested against experimental data and used to estimate the parameters that quantify the motion and are required to calculate the macroscopic, bulk parameters needed in the description of the fluid mechanics of the whole suspension. The model also justifies the rational continuum model for the bioconvection of suspensions of such swimming algae introduced by Pedley & Kessler (1990), thus completing the cycle of modelling from the micro-

scopic behaviour of individual cells to the flow of suspensions containing tens of millions of cells.

Two fundamentally different orientation mechanisms, negative gravitaxis and positive phototaxis have been studied. The former is effected by a passive mechanical torque acting on the asymmetric distribution of mass within the cell as is confirmed by the sinusoidal dependence of the turning angle on the direction of swimming. The latter active mechanism does not depend sinusoidally on the swimming direction but linearly. Further experiments over a complete set of illumination intensities will be required to determine the full range of phototactic behaviour to confirm and quantify the generic responses assumed by Vincent & Hill (1996) in their model of bioconvection driven by phototaxis. These experiments should include recordings of cells swimming in both horizontal and vertical planes.

As discussed in Section 2, the occurrence of thermal drifts is an almost unavoidable feature of this type of experiment. One possible improvement would be to introduce easily identifiable, passively advected particles into the suspension to measure the drifts and cell swimming trajectories simultaneously, so that drifts could be subtracted from the trajectories of the cells before further analysis.

Work is under way, using numerical simulations of biased, correlated random walks, to further understand and quantify the behaviour of the angular

deviations of both the swimming direction and the turning angle of the statistics of the trajectories of swimming micro-organisms on the time step, especially at longer times. The effects of finite pixel resolution and projection are also being studied.

Finally, we hope that this method of analysis will prove a valuable tool for examining the responses of individual algal cells to a whole range of stimuli which elicit taxes.

REFERENCES

ALT, W. & HOFFMANN, G. (1990). *Biological Motion*. Berlin: Springer–Verlag. Lecture Notes in Biomathematics 89.

BATSCHELET, E. (1981). *Circular Statistics in Biology*. London: Academic Press.

BERG, H. C. & BROWN, D. A. (1972). Chemotaxis in *Escherichia coli* analysed by three-dimensional tracking. *Nature* **239,** 500–504.

BOLD, H. C. & WYNNE, M. J. (1978). *Introduction to the Algae. Structure and Reproduction*. New Jersey: Prentice Hall.

BOVET, P. & BENHAMOU, S. (1988). Spatial analysis of animals' movement using a correlated random walk model. *J. theor. Biol.* **131,** 419–433.

CHILDRESS, S., LEVANDOWSKY, M. & SPIEGEL, E. A. (1975). Pattern formation in a suspension of swimming micro-organisms: equations and stability theory. *J. Fluid Mech.* **63,** 591–613.

COX, D. R. & MILLER, H. D. (1965). *The Theory of Stochastic Processes*. New York: John Wiley and Sons Inc.

FISHER, N. I., LEWIS, T. & EMBLETON, B. J. J. (1987). *Statistical Analysis of Spherical Data*. Cambridge University Press.

HÄDER, D. P. & LEBERT, M. (1985). Real time computer-controlled tracking of micro-organisms. *Photochem. Photobiol.* **42,** 509–514.

HILL, N. A., PEDLEY, T. J. & KESSLER, J. O. (1989). Growth of bioconvection patterns in a suspension of gyrotactic microorganisms in a layer of finite depth. *J. Fluid Mech.* **208,** 509–543.

HILL, N. A. & VINCENT, R. V. V. (1993). A simple model and strategies for orientation in phototactic microorganisms. *J. theor. Biol.* **163,** 223–235.

KESSLER, J. O. (1986). Individual and collective fluid dynamics of swimming cells. *J. Fluid Mech.* **73,** 191–205.

KESSLER, J. O., HILL, N. A. & HÄDER, D.-P. (1992). Orientation of swimming flagellates by simultaneously acting external factors. *J. Phycology* **28,** 816–822.

LEBERT, M. & HÄDER, D.-P. (1996). How *Euglena* tells up from down. *Nature* **379,** 590.

LINDSTRÖM, K. (1982). Environment requirement of the dinoflagellate *peridinium cinctum* fa. *westii*. Acta Universitatis Upsaliensis. Abstracts of Uppsala Dissertations from the Faculty of Science 646.

LOVELY, P. S. & DAHLQUIST, F. W. (1975). Statistical measures of bacterial motility and chemotaxis. *J. Theor. Biol.* **50,** 477–496.

MARDIA, K. V. (1972). *Statistics of Directional Data*. London: Academic Press.

PEDLEY, T. J., HILL, N. A. & KESSLER, J. O. (1988). The growth of bioconvection patterns in a uniform suspension of gyrotactic micro-organisms. *J. Fluid Mech.* **195,** 223–237.

PEDLEY, T. J. & KESSLER, J. O. (1990). A new continuum model for suspensions of gyrotactic micro-organisms. *J. Fluid Mech.* **212,** 155–182.

RISKEN, H. (1989). *The Fokker–Planck Equation*. 2nd Edn. Berlin: Springer–Verlag.

VINCENT, R. V. V. & HILL, N. A. (1996). Bioconvection in a suspension of phototactic algae. *J. Fluid Mech.* **327,** 343–371.